







## Article

# Integrated Coastal Zone Management in the Face of Climate Change: A Geospatial Framework for Erosion and Flood Risk Assessment

Theodoros Chalazas <sup>1,2,\*</sup> , Dimitrios Chatzistratis <sup>1</sup> , Valentini Stamatiadou <sup>1</sup> , Isavela N. Monioudi <sup>1</sup> ,  
Stelios Katsanevakis <sup>1</sup>  and Adonis F. Velegrakis <sup>1</sup> 

<sup>1</sup> Department of Marine Sciences, University of the Aegean, University Hill, 81100 Mytilene, Greece

<sup>2</sup> Agrotechnology Unit, Instituut voor Landbouw-, Visserij- en Voedingsonderzoek, Burgemeester Van Gansberghelaan 92, BE 9820 Merelbeke-Melle, Belgium

\* Correspondence: theodoros.chalazas@ilvo.vlaanderen.be

## Abstract

This study presents a comprehensive geospatial framework for assessing coastal vulnerability and ecosystem service distribution along the Greek coastline, one of the longest and most diverse in Europe. The framework integrates two complementary components: a Coastal Erosion Vulnerability Index applied to all identified beach units, and Coastal Flood Risk Indexes focused on low-lying and urbanized coastal segments. Both indices draw on harmonized, open-access European datasets to represent environmental, geomorphological, and socio-economic dimensions of risk. The Coastal Erosion Vulnerability Index is developed through a multi-criteria approach that combines indicators of physical erodibility, such as historical shoreline retreat, projected erosion under climate change, offshore wave power, and the cover of seagrass meadows, with socio-economic exposure metrics, including land use composition, population density, and beach-based recreational values. Inclusive accessibility for wheelchair users is also integrated to highlight equity-relevant aspects of coastal services. The Coastal Flood Risk Indexes identify flood-prone areas by simulating inundation through a novel point-based, computationally efficient geospatial method, which propagates water inland from coastal entry points using Extreme Sea Level (ESL) projections for future scenarios, overcoming the limitations of static ‘bathtub’ approaches. Together, the indices offer a spatially explicit, scalable framework to inform coastal zone management, climate adaptation planning, and the prioritization of nature-based solutions. By integrating vulnerability mapping with ecosystem service valuation, the framework supports evidence-based decision-making while aligning with key European policy goals for resilience and sustainable coastal development.

**Keywords:** Coastal Vulnerability Index (CVI); coastal flood risk; climate adaptation; geospatial analysis; earth observation; multi-criteria decision-making; Integrated Coastal Zone Management (ICZM)



Academic Editor: Fang Yenn Teo

Received: 29 November 2025

Revised: 19 January 2026

Accepted: 20 January 2026

Published: 22 January 2026

**Copyright:** © 2026 by the authors.

Licensee MDPI, Basel, Switzerland.

This article is an open access article distributed under the terms and conditions of the [Creative Commons Attribution \(CC BY\)](https://creativecommons.org/licenses/by/4.0/) license.

## 1. Introduction

Climate change is intensifying at a pace that is already driving widespread disruptions to physical and ecological systems, including the increasing likelihood of crossing multiple climatic tipping points [1,2] and accelerating ocean-related impacts such as warming [3], acidification [4], deoxygenation [5], and biodiversity loss [6,7]. These rapidly unfolding changes are amplifying the frequency and severity of extreme events, reshaping ecosystem

structure and function, and heightening risks to human societies across all regions [8,9]. Coastal zones are among the areas where these climate-driven pressures manifest most acutely, with shoreline erosion and coastal flooding emerging as two of the most pervasive and damaging impacts worldwide [10]. Rising sea levels, intensifying storm regimes, and sediment-supply disruptions facilitate increasing shoreline retreat in many regions, while extreme water levels increasingly threaten flooding of low-lying coastal settlements and infrastructure [11,12]. In the Mediterranean, coastal erosion and flooding already pose large risks to its densely populated coastlines, concentrated tourism economies, and geomorphological sensitivity [13,14]. These dynamics underscore the need for spatially explicit and scalable assessment frameworks capable of capturing both physical susceptibility and socio-economic exposure along the coast. Such frameworks are also required to align with ICZM-based climate adaptation approaches, which emphasize integrated and cross-sectoral coastal planning across multiple governance levels [15].

The concept of vulnerability has become central in coastal risk assessments, particularly in the context of climate-driven threats such as coastal erosion and flooding. Early work in coastal vulnerability assessment introduced composite metrics, commonly referred to as the Coastal Vulnerability Index (CVI), to rank coastal segments according to their susceptibility to change [16,17]. The original CVI formulation combined multiple physical variables, such as geomorphology, shoreline change, coastal slope, relative sea-level rise, wave climate, and tidal range, into a single aggregated index.

Since then, CVI-based approaches have proliferated and diversified, leading to a wide range of indicator selections, aggregation methods, and mapping practices [18–21]. While this diversity has expanded the applicability of vulnerability assessments, it has also reduced methodological comparability and complicated the consistent interpretation of results for cross-regional analysis and policy support.

A systematic review of coastal vulnerability studies found that most assessments are conducted at the local or regional scale, with a strong focus on physical exposure and limited integration of social dimensions or policy relevance [22]. The review also highlighted substantial methodological heterogeneity, including variation in indicator selection, inconsistent weighting and aggregation schemes, and a lack of standardized frameworks, which limits comparability and reproducibility across studies and reduces their applicability for policy-oriented coastal management and ICZM decision-support. Similarly, a more recent meta-analysis of 43 “second-generation” vulnerability index studies emphasized that there is still no consensus on indicator definitions or conceptual dimensions of vulnerability, with many applications continuing to rely heavily on hazard-based or exposure-centric paradigms [23]. Collectively, these reviews underscore a persistent gap between the evolving conceptual understanding of vulnerability, which emphasizes exposure, sensitivity, and adaptive capacity, and its operationalization in coastal vulnerability indices, many of which remain rooted in biophysical assessment traditions.

Recent advances in Earth observation and data-sharing policies have transformed the possibilities for large-scale, consistent coastal assessments [24]. Across Europe, a suite of open-access geospatial infrastructures, such as Copernicus Marine Service [25], the Copernicus Land Monitoring Service [26], and Joint Research Centre datasets [27], offer harmonized physical, environmental, and socio-economic layers at continental scale. These resources provide unprecedented opportunities for implementing Integrated Coastal Zone Management (ICZM) frameworks that are spatially explicit, reproducible, and cross-border comparable. However, recent European assessments indicate that these data infrastructures remain under-utilized in Integrated Coastal Zone Management (ICZM) and Maritime Spatial Planning (MSP) practices. Persistent barriers include fragmented data provision driven by institutional and technical inconsistencies, such as differences in data ownership,

formats, spatial resolution, and update cycles, as well as limited awareness and capacity among practitioners to track rapidly evolving data infrastructures and methodologies. Together, these factors contribute to a lack of harmonized geospatial data frameworks at the regional level, limiting the effective integration of open-access datasets into ICZM applications [28]. This study introduces an ICZM-oriented geospatial framework that advances coastal risk assessment in three specific ways. First, it jointly evaluates coastal erosion vulnerability and coastal flood exposure within a single, internally consistent methodology applied at the national scale, defined as spatially continuous, wall-to-wall coverage using harmonized datasets, standardized spatial units, and uniform analytical workflows across the entire coastline. Second, socio-economic dimensions, including land use, population exposure, recreational economic value, and accessibility-related benefits, are explicitly incorporated as normalized indicators within the index construction, where they are aggregated alongside physical variables to form composite socio-economic importance and overall vulnerability scores. This approach ensures that human use and coastal services directly influence the resulting risk patterns, rather than being treated as ancillary overlays. This allows human use and coastal services to directly influence vulnerability and exposure patterns. Third, by relying exclusively on harmonized, open-access European datasets and standardized geospatial workflows, the framework supports reproducible and transferable assessments that facilitate cross-regional comparison, prioritization, and transparent communication, key operational requirements of ICZM. Together, these features address a well-recognized limitation in existing coastal assessments, namely the lack of spatially consistent, scalable screening tools that integrate physical and socio-economic dimensions to support strategic climate adaptation planning at higher governance levels.

In this context, this study develops a dual-framework geospatial methodology for coastal risk assessment, demonstrated through a national-scale case study along the Greek coastline. The framework consists of two complementary components designed to reflect the distinct spatial scales and impact pathways of coastal erosion and coastal flooding. Coastal erosion vulnerability is assessed through the Coastal Erosion Vulnerability Index (CEVI), applied at the beach scale, where erosion processes directly affect sediment dynamics, ecosystem services, and socio-economic uses concentrated within discrete beach units. In contrast, coastal flooding is assessed through Coastal Flood Risk Indices (CFRI) applied to low-elevation coastal segments, capturing the broader spatial extent over which sea-level rise and extreme sea-level events affect infrastructure, settlements, and population exposure. Although CEVI and CFRI are calculated separately, the framework is designed to present erosion vulnerability and flood exposure within a common ICZM-oriented structure, enabling their coordinated interpretation for national-scale screening, comparison, and prioritization, rather than their aggregation into a single composite metric. The use of different spatial units reflects the dominant spatial manifestation of each hazard, while maintaining comparability through the use of harmonized datasets and standardized analytical workflows applied consistently across the entire coastline.

Greece provides a representative and policy-relevant setting to pilot this framework. A large proportion of the country's population, infrastructure, and economic activity is concentrated along its approximately 16,000 km coastline, which encompasses a wide range of geomorphic settings, including mainland sandy beaches, rocky shores, low-lying deltas, and numerous islands. Previous assessments indicate that Greek beaches and low-elevation coastal systems are already experiencing significant erosion and increasing exposure to extreme sea-level events, with these pressures expected to intensify in coming decades [29,30]. These characteristics make Greece a suitable test case for evaluating an ICZM-aligned, national-scale framework under heterogeneous coastal conditions and governance contexts common across the Mediterranean region.

2. Methodology

The approach adopted in this study is based on the integration of open-access spatial explicit datasets and reproducible, scalable geospatial methodologies. These datasets span physical variables (such as wave power and shoreline erosion), ecological variables (including the cover of seagrass meadows), and socio-economic indicators (notably land use, population distribution, and recreational value). An overview of the methodological workflow and its two-phase structure is provided in Figure 1. All input datasets were harmonized through reprojection to a common European spatial reference system (EPSG:3035–ETRS89/LAEA Europe) to ensure spatial consistency and interoperability across layers. For visualization purposes and alignment with global geospatial conventions, final outputs were displayed in the EPSG:4326 (WGS 84) coordinate reference system. The geospatial workflow combined a suite of advanced techniques and tools, implemented primarily in QGIS 3.44 and a Python 3.10 environment. Buffering operations were conducted to define zones of influence around each beach unit or coastal segment. Point-based datasets were spatially matched to beach polygons through nearest-neighbor analysis, ensuring that each polygon was assigned the most geographically relevant value based on proximity and dataset resolution. Quantitative attributes extracted from these buffers or point assignments were further normalized, classified, and combined using zonal statistics, field calculations, and spatial joins.

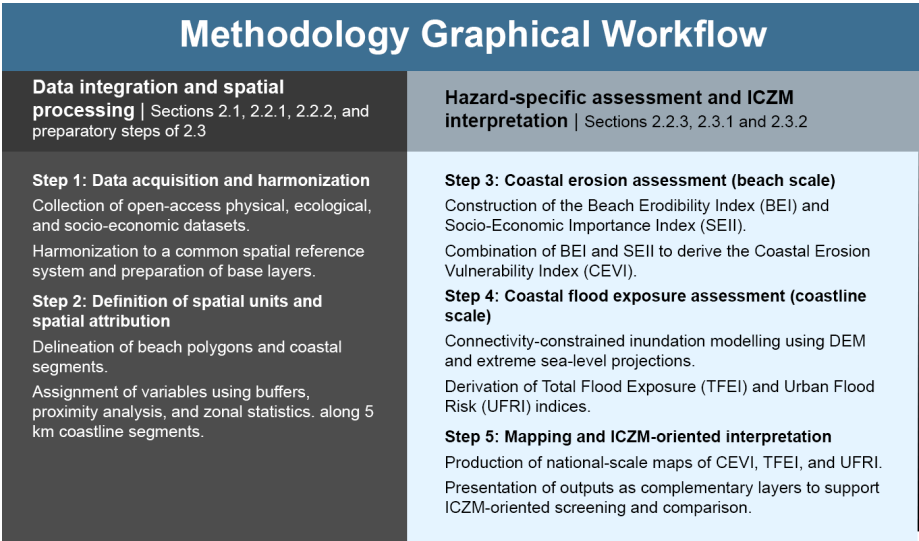


Figure 1. Methodological graphical workflow.

In the flood risk component of the analysis, coastal elevation data (DEM) were processed into millions of point features, each attributed with local elevation and projected extreme sea level values for 2050 under RCP 8.5. A custom Python-based algorithm was developed to propagate flooding inland using a proximity approach. Flood propagation was constrained by topographic connectivity, such that inland low-elevation points lacking continuous hydraulic connection to the shoreline were excluded, thereby reducing false-positive inundation typical of static bathtub approaches. Further geospatial analysis was used to associate flooded points with urban zones and to summarize affected points within fixed 5 km coastal segments, a pragmatic reporting scale chosen to balance spatial detail with interpretability and to support national-scale screening and comparison of flood exposure patterns. These spatial aggregations supported the development of two complementary coastal flood risk metrics: the Total Flood Exposure Index (TFEI), capturing overall inundation along the coastline, and the Urban Flood Risk Index (UFRI), quantifying exposure specifically within built-up areas. In comparison, the erosion component of the

framework operates at the beach-unit scale and consists of (i) the Beach Erodibility Index (BEI), which integrates physical and ecological drivers of shoreline susceptibility, and (ii) the Socio-Economic Importance Index (SEII), which represents human and economic exposure at each beach. The combination of these two indices forms the Coastal Erosion Vulnerability Index (CEVI). By separating the beach-scale erosion indices (BEI, SEII, CEVI) from the coastline-scale flood exposure indices (TFEI and UFRI), the framework preserves the distinct hazard dynamics, spatial logics, and management implications of each threat. Rather than being combined, erosion and flooding indices are intended to be interpreted jointly as complementary layers within an ICZM screening framework, enabling decision-makers to distinguish locations dominated by chronic shoreline retreat from those primarily exposed to episodic inundation, or affected by both hazards simultaneously.

### 2.1. Data and Materials

This study relies exclusively on harmonized, open-access geospatial datasets and reproducible analytical workflows. Physical and environmental inputs include offshore wave characteristics from the Copernicus Marine Environment Monitoring Service (CMEMS), historical shoreline change and projected coastal erosion from Joint Research Centre (JRC) LISCOAST datasets, extreme sea-level projections for future scenarios from the JRC, coastal land cover from the Copernicus Coastal Zones Land Cover/Land Use dataset, high-resolution elevation data from the Copernicus DEM, and seagrass meadow distribution from open-access national habitat inventories. Socio-economic inputs include population data from the Global Human Settlement Layer (GHSL), land-use composition from Copernicus land-cover products, and recreational use indicators derived from survey data, official tourism statistics, and openly accessible georeferenced social-media metadata.

All external datasets used are freely accessible through European open-data infrastructures. Detailed dataset descriptions, links, and references are provided in the relevant sections of Section 2 where each dataset is introduced and applied. All derived datasets and indices produced in this study are made available through the Data Availability section to ensure transparency, reproducibility, and reuse.

### 2.2. Coastal Erosion Vulnerability

To evaluate beach vulnerability along the Greek coastline, we developed a geospatial framework that integrates both natural and human-related factors influencing erosion susceptibility and coastal exposure. This dual structure captures the interaction between physical drivers of shoreline change and the socio-economic significance of the affected areas. Integration of physical and socio-economic indicators is implemented through a multi-criteria decision analysis, involving normalization of all variables, application of predefined weights, and aggregation based on distance to ideal and anti-ideal solutions (see Section 2.2.3 for details). The approach focuses on identified beach polygons and combines environmental data, geomorphological trends, and socio-economic attributes into a consistent, spatially explicit assessment. By analyzing both the inherent susceptibility of beaches to physical processes and the value of assets at risk, the framework supports targeted adaptation strategies and coastal management decisions. Polygonal representations of beaches were extracted from the Copernicus Coastal Zones Land Cover/Land Use 2018 (CLC) dataset [31] by selecting features classified as “beaches, dunes, and sand plains” (CLC class 331), which meet the dataset’s minimum spatial thresholds ( $\geq 0.5$  ha area and  $\geq 10$  m width). While the CLC minimum mapping unit limits the representation of very small or highly fragmented beaches, the dataset provides harmonized, wall-to-wall national coverage of beach-related landforms across Greece. The resulting ~2100 beach polygons therefore represent consistently mapped, nationally comparable beach units suitable for



first-order erosion vulnerability assessment; their representativeness and limitations are evaluated in the Discussion. The use of harmonized, open-access European datasets was central to the framework's reproducibility and scalability. Such datasets enable spatially consistent assessments across administrative boundaries, allowing coastal segments to be evaluated using the same indicators, assumptions, and spatial resolution. This consistency is particularly relevant for ICZM, which requires comparable information across regions to support strategic planning, prioritization, and coordination among authorities operating at different governance levels. By leveraging this shared geospatial infrastructure, the framework supports transparent, repeatable, and cross-border comparable assessments aligned with European ICZM policy objectives [32,33].

### 2.2.1. Natural Environment

The natural environment component of the CEVI focuses on the physical and ecological factors that influence beach erodibility. This includes wave power, historical shoreline retreat, projected erosion under climate change scenarios, and the cover of protective submerged vegetation (e.g., *Posidonia oceanica*). These variables were selected because they capture both the beach erosion forcing (e.g., wave energy) and its intrinsic resistance to erosion (e.g., through vegetative stabilization). Together, they describe the natural dynamics that shape coastal geomorphology. Each variable was spatially assigned to individual beach polygons using proximity-based geospatial analysis, ensuring that every beach was linked to relevant physical conditions. The combination of these layers forms the BEI, which quantifies the intrinsic physical vulnerability of each beach to erosive forces.

#### Wave Energy

Wave energy is a primary driver of coastal erosion and an essential component of coastal vulnerability assessments. To represent this, we derived wave power values using the Copernicus Marine Environment Monitoring Service (CMEMS) MED-SEA\_MULTIYEAR\_WAV\_006\_012 product [34], which provides high-resolution wave height and period data for the Mediterranean Sea. From this dataset, we extracted all available points covering the Greek maritime area for the year 2024. Wave power in this study is not intended to represent long-term wave climatology or to provide predictive estimates of site-specific nearshore forcing. Instead, it is used as a relative indicator of exposure to energetic wave conditions at national scale, enabling comparison of spatial contrasts in wave-driven erosive potential along the coastline. Under this screening objective, the analysis assumes that large-scale spatial patterns in wave exposure around Greece are broadly persistent, even though absolute wave energy varies interannually.

To characterize energetic wave conditions most relevant for coastal impacts, we applied a statistical threshold by retaining only the 90th percentile of significant wave heights at each point. This percentile was selected to emphasize recurrent high-energy wave conditions that exert a dominant control on beach morphodynamics, rather than average wave climate or rare extreme events [35]. For those events, we then extracted the corresponding wave periods and computed wave power ( $P$ ) using the deep-water wave energy flux formula:

$$P = \frac{\rho g^2}{64\pi} H_{m0}^2 T_e \approx 0.5 H_{m0}^2 T_e \quad (1)$$

where  $P$  the Wave energy flux (kW/m),  $H_{m0}$  the Significant wave height (m),  $T_e$  the Energy period (s),  $\rho$  the Water density (typically 1025 kg/m<sup>3</sup> for seawater) and  $g$  the Gravitational acceleration (9.81 m/s<sup>2</sup>).

For each point, we calculated the mean wave power based on these high-energy conditions across the year, resulting in a spatial distribution of extreme wave forcing around Greece. Using geospatial analysis, we then selected the points closest to the

coastline to represent wave conditions most likely to impact the shore. Each beach polygon was assigned the nearest available wave power value through geospatial proximity analysis. This nearest-point assignment does not resolve nearshore wave transformation processes (e.g., refraction, shoaling, breaking, or shoreline orientation). Resolving these processes consistently at national scale would require detailed bathymetry and computationally intensive modeling; therefore, offshore wave power is used as a simplified, physically based proxy of relative wave exposure, prioritizing spatial consistency and reproducibility over local-scale physical realism. This variable serves as a key indicator of external erosive forcing in the CEVI, providing a physically based measure of the intensity of wave-driven energy that contributes to coastal dynamics.

### Historical Erosion

To quantify historical erosion pressure on Greek beaches, we incorporated data from the Global Long-Term Shoreline Evolution dataset [36] developed by the Joint Research Centre (JRC) under the LISCOAST (Large Scale Integrated Sea-level and Coastal Assessment Tool) initiative. This dataset provides a global assessment of shoreline movement derived from satellite imagery between 1984 and 2015, estimating over 28,000 km<sup>2</sup> of land loss worldwide, nearly double the area gained through accretion. The dataset captures the geomorphic footprint of both natural processes and anthropogenic pressures and is particularly useful for assessing long-term erosion trends. We extracted values for shoreline retreat by identifying the nearest transect point to each beach polygon along the Greek coastline. To maintain a conservative focus on vulnerability, we only considered cases where retreat was observed. In all other cases (stable or accreting shorelines), we assigned a value of zero, indicating no erosion contribution to the erodibility index. This method ensures that only areas historically affected by shoreline retreat are weighted in the physical vulnerability assessment.

### Projected Erosion

To incorporate future shoreline retreat into the erodibility index, we used data from the JRC Global Coastal Erosion Projections. Projected shoreline retreat is derived from the sandy-coast erosion dataset of Voudoukas et al. [37] which represents coastal evolution as the combined effect of sea-level-rise-driven retreat, ambient shoreline change, and short-term storm-driven erosion. The sea-level-rise-driven component reflects the long-term response of sandy coastlines to projected eustatic sea-level rise under different climate scenarios. The ambient shoreline-change component is obtained by extrapolating observed shoreline trends over the 1984–2015 period and therefore implicitly incorporates the cumulative effects of geological processes, sediment supply variations, and human interventions. Short-term storm-driven erosion accounts for episodic shoreline retreat associated with extreme wave events. The resulting estimates reflect potential shoreline displacement under different climate change scenarios and time horizons, expressed as signed shoreline position change (in m), where negative values indicate erosion and positive values indicate shoreline advance (accretion).

In our study, we selected the RCP 8.5 scenario for the year 2100, using the 95th percentile values to reflect high-end projected erosion. The use of RCP 8.5 and 95th percentile projections reflects a high-end scenario choice aligned with national-scale vulnerability screening, rather than an estimate of most-likely future shoreline change. Only negative values (representing shoreline retreat) were considered in the analysis, while positive or neutral values were treated as zero. These erosion values were spatially assigned to each beach polygon based on the nearest coastal segment in the dataset. This approach provides a future-oriented indicator of erosion risk, complementing the historical shoreline

retreat variable while focusing specifically on erosional pressure. It is important to note that this method does not account for potential accretion or stability, and thus reflects a unidirectional assessment of vulnerability. These shoreline-change projections have become a reference dataset for large-scale erosion modeling and coastal-risk analysis. Their applicability at national scales has been demonstrated to assess coastal adaptation and migration dynamics with high spatial resolution [38]. Similar applications at continental and global levels [39,40] have also demonstrated the dataset's reliability and scalability, supporting its use here for consistent, reproducible national-scale erosion-vulnerability assessment.

#### Seagrass Meadows Cover

To represent the protective role of submerged vegetation in coastal erosion processes, we included the percent cover of seagrass meadows as one of the variables in the erodibility index. Data were obtained from the open-access dataset "Seagrass Meadows in the Greek Seas" [41,42]. This dataset was created using a combination of satellite imagery and side-scan sonar, underwater video, and other field observations, and provides a detailed spatial distribution of seagrass habitats along the Greek coastline. *Posidonia oceanica* is the dominant species, occupying shallow coastal zones where it forms dense meadows known to significantly reduce wave energy and stabilize sediments [43]. We used a 1 km buffer to represent the nearshore zone where meadows can occur and influence sediment dynamics; *P. oceanica* meadows commonly extend to ~40 m depth [44]. Given that Greek nearshore slopes are frequently on the order of ~0.02–0.04 slope [45], a 1 km distance corresponds approximately to ~20–40 m depth, providing a pragmatic national-scale proxy while acknowledging that local slope variability can shift the effective depth represented by a fixed buffer. Seagrass meadows are considered a critical natural defense against coastal erosion, acting as biological breakwaters that dissipate wave energy, trap sediments, and reduce longshore transport; their occurrence is associated with increased seabed stability and reduced coastal retreat rates [46,47]. Therefore, including seagrass cover adds a key ecological parameter to the erodibility index, acknowledging the role of natural ecosystems in buffering human and climate-induced pressures on beaches.

#### 2.2.2. Human Environment

To assess the socio-economic dimension of coastal vulnerability, we developed indicators that reflect both population exposure and the intensity of human use in the immediate beach hinterland. Socio-economic variables were spatially summarized at the beach polygon scale using variable-specific buffer zones designed to represent the functional backshore and adjacent areas of influence relevant to each indicator (e.g., residential exposure, land use, and tourism activity). All variables were normalized and integrated using an unweighted TOPSIS-based multi-criteria decision analysis framework, in which indicators contribute equally and are aggregated through their distance to ideal and anti-ideal solutions. The selected variables aim to capture the types of assets and activities most likely to be affected by erosion and flooding, including land uses, residential population, and tourism-related economic value. Each variable was spatially summarized at the beach polygon scale, using tailored buffer zones to reflect the functional backshore and adjacent areas of influence. This ensures that human pressures are directly linked to the physical units of analysis. These variables jointly inform two distinct outputs: the Human Environment component of the CEVI, and the SEII, which highlights areas of concentrated recreational, residential, or economic value. This dual perspective enables both risk prioritization and value-based planning, supporting more informed decisions for sustainable coastal management.



### Land Use Vulnerability Index

To quantify the socioeconomic exposure of the beach immediate hinterland, we assessed land use composition within a 100 m inland buffer extending from the landward boundary of each beach polygon. We selected a 100 m buffer to focus specifically on the proximal backshore zone, which contains built environment, agricultural activities, and natural features that most directly influence or are impacted by beach erosion and coastal flooding. The 100 m buffer is intended as a functional backshore screening unit rather than a process-based impact zone, capturing land uses most directly adjacent to the shoreline and thus most immediately exposed at national scale. By limiting the analysis to this narrow strip of land immediately adjacent to the beach, we ensured the vulnerability assessment targeted areas with high likelihood of impacts. Buffers were clipped to the landward side to exclude open water and measured using geospatial analysis. We employed again the CLC coastal dataset, reclassifying land cover codes into four groups: artificial/urban areas, agricultural areas, natural and forested areas, and wetlands/water bodies. Within each buffer, we calculated the total buffer area and the areas occupied by each reclassified land use group. We then derived the normalized fractional coverage (0–1) for each class by dividing its area by the total buffer area, ensuring fractions summed to one. Vulnerability weights were assigned to each class based on their potential socioeconomic exposure to coastal hazards: 1 for urban areas, reflecting maximum vulnerability due to the high concentration of people, infrastructure, and economic assets directly at risk from coastal erosion/flooding; 0.7 for agricultural areas, representing significant economic exposure through potential loss of crops and farmland, albeit with typically lower population density; 0.3 for natural and forested areas, assuming limited direct socio-economic exposure but also vulnerability due to potential loss of ecosystem services; and 0 for wetlands and water bodies, which although do not contain human population and/or assets but they, nevertheless, provide protection from erosion/flooding and reduce overall vulnerability. The assigned land-use weights are expert-defined and intentionally configurable, allowing users to adapt the index to different management priorities or policy contexts. A land use vulnerability index was then computed for each beach polygon as the weighted sum of these normalized fractions, providing a robust measure of socio-economic exposure directly related to the spatial distribution of land uses in the immediate backshore.

### Population Exposure Assessment

To assess population exposure as a component of coastal vulnerability, we calculated the total residential population within a 500 m buffer surrounding each beach polygon. The population data were obtained from the Joint Research Centre (JRC) GHSL-POP dataset [48], which provides global gridded population estimates at 100 m resolution. We used a 500 m inland buffer to capture proximal population exposure, consistent with its use in large-scale coastal exposure assessments where fixed buffers facilitate reproducible, comparative analysis across extensive coastlines [40]. We used the most recent available five-year interval to ensure contemporary relevance. For each beach, the buffer was generated outward from the beach polygon, and all population values falling within this 500 m zone were summarized to provide a total population count associated with that beach. Population is a critical variable in both the Socioeconomic Importance Index and the broader Coastal Vulnerability Index, as it directly reflects the potential human exposure to coastal erosion/flooding. Beaches surrounded by densely populated areas are at higher risk of having people affected during erosion or flooding events, and they also represent greater stakes in terms of emergency response, health impacts, and economic disruption.

### Recreational Use Value

To quantify recreational beach use as a socio-economic variable, we combined primary survey data, official tourism expenditures, and crowdsourced visitation proxies, and mapped the resulting values to individual beaches. The workflow follows two distinct steps: (i) economic valuation and (ii) spatial allocation (mapping) [49]. Economic use values were estimated from (i) domestic day-trip spending and travel costs reported in a structured survey of Greek residents ( $n = 527$ ; March 2023–February 2024, stratified by age group and extrapolated to the population of each group [50]), and (ii) inbound tourism receipts from the Bank of Greece's sample-based border surveys [51], seasonally adjusted to isolate May–September sun-and-beach revenues by subtracting the October–April average of non-coastal recreation. The components were estimated independently and expressed in the same unit (€/year), enabling additive aggregation without arbitrary cross-source weighting. Spatial distribution was based on a visitation index constructed from Flickr API metadata (geotagged uploads near each beach centroid, 2005–2022) [52]. Average annual photo counts were normalized to a 0–1 scale (national sum = 1) and used to allocate domestic, inbound, and conservation values to each beach, expressed per hectare (€/ha/yr). Recreational beach use is included as a dedicated socio-economic layer because it captures actual demand and concentration of benefits at specific sites. In Greece, where Sun, Sand and Sea tourism underpins local livelihoods and coastal services [53,54], this metric links hazard signals (erosion and flooding) to potential disruption of tourism-driven benefits and complements exposure variables by identifying beaches where socio-economic stakes are highest.

### Wheelchair User Value

To quantify recreational beach use for wheelchair users as a socio-ecological variable, we combined primary survey data, monetary valuation, and crowdsourced/accessibility infrastructures proxies and mapped the resulting values to individual beaches. The workflow follows two distinct steps: (i) economic valuation and (ii) spatial allocation (mapping). Direct use value was estimated from reported expenditures on overnight and day trips collected through an online survey of wheelchair users (Mar–Jun 2024), and extrapolated to the estimated population of Greek wheelchair users [55]. Spatial distribution followed a hierarchical allocation based on stated visitation preferences: first distinguishing beaches with and without accessible infrastructure, and then weighting specific feature types (e.g., ramps/sea-entry systems, designated parking, accessible toilets, adapted changing rooms, shaded areas, accessible showers). Within each category, a visitation index was constructed from Flickr API metadata (geotagged uploads, 2005–2022), and normalized annual photo counts allocated total recreational value across beaches. Final values were expressed per hectare (€/ha/yr). Wheelchair-user recreation is included as a separate socio-ecological layer because accessibility depends on the availability and operability of dedicated solutions, which are sensitive to geomorphology and hazard conditions (shoreline retreat, beach narrowing, storm run-up, inundation). These benefits are not captured by general recreation or population metrics. By incorporating both visitation (demand) and accessible infrastructure (usability), the layer links hazard to an equity-relevant valuation and informs the resilient siting and deployment of accessibility features.

#### 2.2.3. Key Beach Indices

To support spatially targeted adaptation and planning decisions within the framework of ICZM, three composite indices were developed, focusing specifically on beach systems: the BEI, the SEII, and the CEVI. These indices were computed at the scale of individual beach polygons, delineated from high-resolution Copernicus land cover data,

and designed to capture both the physical susceptibility and the socio-economic significance of Greece's beaches. By operating at this scale, the framework provides a spatially explicit understanding of vulnerability where environmental hazards and human uses most directly interact.

The BEI characterizes the physical susceptibility of each beach to erosive processes. It includes four indicators: offshore wave power (as a proxy for external hydrodynamic forcing), historical shoreline retreat (capturing long-term geomorphological change), projected shoreline retreat under high-end climate scenarios (anticipating future impacts), and Seagrass meadow cover (serving as a natural buffer). The SEII evaluates the human and economic stakes associated with each beach. This includes land use vulnerability, residential population, recreational beach use value, and wheelchair-user specific value. Together, these variables describe the intensity, diversity, and distribution of human uses that could be affected by erosion or flooding at each beach site.

The CEVI combines both the erodibility and socio-economic importance indices to provide a balanced, site-specific measure of beach vulnerability. This integrated score supports ICZM by highlighting priority areas for intervention, where both environmental degradation and social disruption risks are high. By focusing the analysis at the beach polygon level, the indices offer a fine-grained and spatially explicit tool for national and local decision-makers tasked with managing erosion, safeguarding coastal assets, and allocating resources efficiently.

All indices were constructed using the Technique for Order of Preference by Similarity to Ideal Solution (TOPSIS), a multi-criteria decision-making (MCDM) method that allows consistent comparison across multiple variables and spatial units [56]. TOPSIS was selected because it provides a transparent, non-compensatory framework for ranking spatial units based on their relative proximity to idealized best and worst conditions. TOPSIS does not require pairwise comparisons or subjective preference matrices, making it well suited for large-scale, data-driven screening applications. In this framework, each beach polygon was treated as a decision unit characterized by a set of normalized variables representing its physical, ecological, or socio-economic attributes. The normalization of variables ensures comparability across different magnitudes and units, expressed as:

$$a_{ij} = \frac{x_{ij}}{\sqrt{\sum_{k=1}^n x_{ik}^2}} \quad (2)$$

where  $x_{ij}$  is the raw value for region  $i$  and variable  $j$ .

Two reference points were then established for each criterion: the **positive ideal solution**  $A_j^+$  representing the most favorable (best) value, and the **negative ideal solution**  $A_j^-$  representing the least favorable (worst) value. For beneficial variables, where higher values reduce vulnerability (e.g., seagrass meadow cover, which stabilizes sediments), these are defined as:

$$A_j^{+max\{a_{ij}\}} \text{ and } A_j^- = \min\{a_{ij}\} \quad (3)$$

For non-beneficial variables, where higher values increase vulnerability (e.g., wave power, historical and projected erosion), the roles are reversed.

The Euclidean distance of each beach from the positive and negative ideals was then computed as:

$$d_i^+ = \sqrt{\sum_{j=1}^m (a_{ij} - A_j^+)^2} \text{ and } d_i^- = \sqrt{\sum_{j=1}^m (a_{ij} - A_j^-)^2} \quad (4)$$

The TOPSIS Closeness Coefficient (CC), which expresses the relative performance of each beach, was then calculated as:

$$CC_i = \frac{d_i^-}{d_i^+ + d_i^-} \quad (5)$$

Higher  $CC_i$  values indicate closer proximity to the ideal solution, representing lower physical vulnerability or higher beneficial performance. To ensure interpretability and consistency across indices, the erodibility coefficients were reversed, so that values closer to 1 indicate greater vulnerability. This post-processing step allows all resulting indices to share a common scale and meaning, facilitating comparison and integration, a sign convention applied to ensure that higher index values consistently represent higher vulnerability across all indices. This process yielded composite scores representing the relative erodibility, socio-economic significance, and overall vulnerability of each beach. Equal weights were adopted to avoid introducing additional subjectivity in the absence of defensible evidence for prioritizing specific drivers at national scale, and to ensure that all physical and socio-economic dimensions contribute symmetrically to the vulnerability assessment. The modular structure of the framework allows users to modify variable weights in future applications to reflect local priorities, management objectives, or stakeholder preferences.

### 2.3. Coastal Flood Exposure Risk

As part of a comprehensive assessment of coastal vulnerability, we developed a national-scale analysis of flood exposure focusing on low-lying coastal zones vulnerable to future sea level rise. While beach-scale indices address erosion susceptibility and socio-economic value, this component expands the spatial scope to identify areas at risk of marine inundation across the entire Greek coastline. The method combines established sea level rise projections with topography-based modeling to simulate coastal flooding in 2050 under a high-impact climate scenario. This analysis enables the identification of priority zones for flood resilience measures, infrastructure planning, and long-term adaptation under ICZM strategies.

#### 2.3.1. Coastal Flood Exposure Modeling Under Future Sea Level Rise

To assess flood exposure along the Greek coastline under future sea level rise scenarios, we developed a high-resolution, spatially explicit inundation model grounded in digital elevation data and probabilistic projections of extreme sea levels (ESLs) for 2050. This analysis focuses on identifying low-lying coastal zones likely to be inundated under climate-driven sea level rise, offering crucial spatial insights for coastal risk management and planning. Many national-scale coastal flood assessments rely on simplified “bathtub” models, which delineate inundation solely based on areas below a given water level threshold, without accounting for topographic connectivity [57]. While computationally simple and widely used in large-scale assessments, static ‘bathtub’ models tend to overestimate flood extents, particularly in low-lying and flat terrain where water flow processes are not properly represented [58]. To reduce such biases, we employed an enhanced bathtub approach that incorporates terrain connectivity, providing more realistic estimates of inundation while maintaining scalability for national-level analysis [59].

The foundation of this geospatial model was a high-resolution elevation point cloud (~4 million points) derived from the Copernicus DEM GLO-30, a harmonized 30 m resolution digital elevation model covering Europe [60]. To restrict the analysis to areas with plausible exposure to marine flooding, the DEM was first masked to a 1000 m inland buffer from the coastline, which was extracted from the CLC Coastal Zones 2018 layer. The resulting clipped raster was then converted into a structured point cloud, with each

point carrying geographic coordinates and surface elevation. We overlaid this elevation dataset with projected 2050 Extreme Sea Level (ESL) values, incorporating tidal dynamics, storm surge, and mean sea level rise under the high-end RCP 8.5 scenario, sourced from the JRC of the European Commission [61]. The analysis began by flagging all elevation points with values below their corresponding ESL projections, representing potential flood-prone locations. We selected the high-end RCP 8.5 scenario for 2050 to adopt a precautionary, stress-testing perspective suitable for coastal risk assessment. Although recent IPCC AR6 assessments indicate that high-emission pathways are now considered low likelihood under current policy trends [62], they remain relevant for evaluating the worst potential impacts and related adaptation planning. Moreover, mid-century sea-level projections show limited divergence between high-end and intermediate scenarios, with RCP 8.5 closely tracking pathways such as SSP2-4.5 through 2050 [63–65], making it an appropriate choice for near-term exposure modeling. At present, SSP-based extreme sea level projections are not yet available in the operational datasets used in this study (e.g., JRC coastal impact projections), necessitating the use of RCP scenarios for consistency with available inputs.

Flooding was initiated only from shoreline-adjacent entry points, identified as the points closest to the coastline extracted from the CLC Coastal Zones 2018 dataset. From each entry point, a 40 m neighborhood search was performed to identify adjacent points that were both lower in elevation and below the ESL threshold. If these conditions were met, the point was marked as flooded, and the search continued iteratively outward, allowing flood spread only along hydrologically connected pathways. This approach prevents the overestimation typical of planar models by excluding isolated inland depressions that lack hydraulic connectivity to the coast. The result is a more physically plausible spatial footprint of marine inundation under future conditions. The final product, a spatially explicit georeferenced point dataset, identifies areas along the Greek coastline projected to be inundated under 2050 sea level rise scenarios. The 40 m neighborhood distance was selected to ensure connectivity between adjacent DEM cells given the 30 m resolution of the Copernicus GLO-30 DEM, while the 1000 m inland mask was applied as a pragmatic national-scale constraint to capture coastal flood-prone zones while maintaining computational efficiency; neither parameter is intended as a calibrated physical flood limit.

### 2.3.2. Index Construction and Urban Risk Prioritization

To translate the point-based flood projections into actionable spatial metrics, we developed two complementary indices that capture total flood exposure and urban-specific flood risk across the Greek coastline. These indices enable prioritization of adaptation and planning efforts within the framework of ICZM, by highlighting areas where marine inundation intersects with population centers and critical infrastructure. First, the national coastline was segmented into uniform 5 km linear units. Using the shoreline geometry extracted from the CLC Coastal Zones 2018, each 5 km segment was paired with a corresponding inland polygon extending 500 m landward from the coastline, producing a series of standardized 5000 m × 500 m rectangular analysis units. These polygons represent the immediate coastal fringe most vulnerable to marine inundation and socio-economic disruption. For each segment, we calculated the TFEI by spatially joining the projected flood points (derived from the geospatial propagation model described in Section 2.2.1) with the inland polygons. The number of flooded points falling within each segment's inland polygon was divided by the total number of elevation points in that polygon, producing a percentage of land area projected to be inundated under 2050 sea-level-rise conditions. This metric reflects general flood exposure across the entire coastal interface, accounting for variations in topography, coastal morphology, and ESL projections.



To complement this assessment, we developed an Urban Flood Risk Index that focuses on the exposure of built environment. The UFRI was calculated by identifying the flooded points that fell within urban land-use areas from the CLC Coastal Zones 2018 dataset. These urban areas were spatially intersected with the 5 km coastal segments, and the number of flooded points within these urban polygons was used to estimate the flooded urban area. This was then divided by the total area of each 5 km coastal segment to produce a consistent percentage of total land area affected by urban flooding. This metric serves as a proxy for socio-economic and infrastructural vulnerability, highlighting segments where flood impacts intersect directly with human settlements and assets. Together, these two indices offer complementary perspectives: the Total Flood Exposure Index captures geophysical vulnerability across the entire coastal zone, while the Urban Flood Risk Index emphasizes the exposure of critical built assets. Both were normalized on a 0–1 scale and can be used independently or combined for multi-criteria prioritization in national coastal resilience planning.

### 3. Results

#### 3.1. Natural and Human Environment: Spatial Distribution

Wave energy (Figure 2a) displays pronounced regional variability across the Greek coastline, reflecting the combined influence of coastal geomorphology, wind regimes, and wave fetch. The highest values (22–37 kW m<sup>−1</sup>) occur predominantly along the northern, northwestern, and western Crete, where long open-water fetches toward the Aegean and Mediterranean basins produce consistently energetic waves. Elevated wave energy also characterizes several parts of the central and southern Aegean, especially around the central and southeastern Aegean islands (Cyclades, Skyros, Southern Rhodes), as well as the northern Aegean. Seagrass cover (Figure 2b) exhibits a mixed, but spatially coherent distribution across Greece, with high-density areas occurring in both mainland and island regions. The largest and most continuous patches are found along the Chalkidiki peninsulas and the northeastern coastline, as well as the northeastern Aegean islands (Limnos and Lesvos). Substantial cover is also present along southern and eastern Attica, forming one of the most prominent mainland seagrass zones. Additional areas of high cover are observed along sections of the western Greek coastline. Historical shoreline retreat (Figure 2c) shows several well-defined high-erosion sectors across Greece. The highest values are concentrated in Crete, especially along its northern coastline, where retreat is widespread and persistent. Consistently elevated values also appear at the Chalkidiki peninsula and the northeastern Aegean coast. Additional high-retreat segments appear along the coast of the western Peloponnese and northwestern mainland Greece, probably reflecting the Ionian coast open setting. Localized hotspots are also visible on several Aegean islands. By comparison, sheltered bays and much of the coast of the central Greece show no or limited historical retreat. Projected shoreline retreat (Figure 2d) under the high-end scenario shows a spatial pattern that reinforces and expands several of the historical erosion hotspots. Crete again displays some of the highest projected coastal retreat values, particularly along its northern and northeastern coasts. Elevated projections are also evident across the Chalkidiki peninsulas and the Thrace–northern Aegean sector. Distinct high-retreat signals appear on Limnos and parts of Lesvos. Additional high values are present along the western Peloponnese [14]. Overall, the projected erosion map indicates that many of the regions historically affected by retreat are expected to experience continued or intensified shoreline displacement through the end of the century.

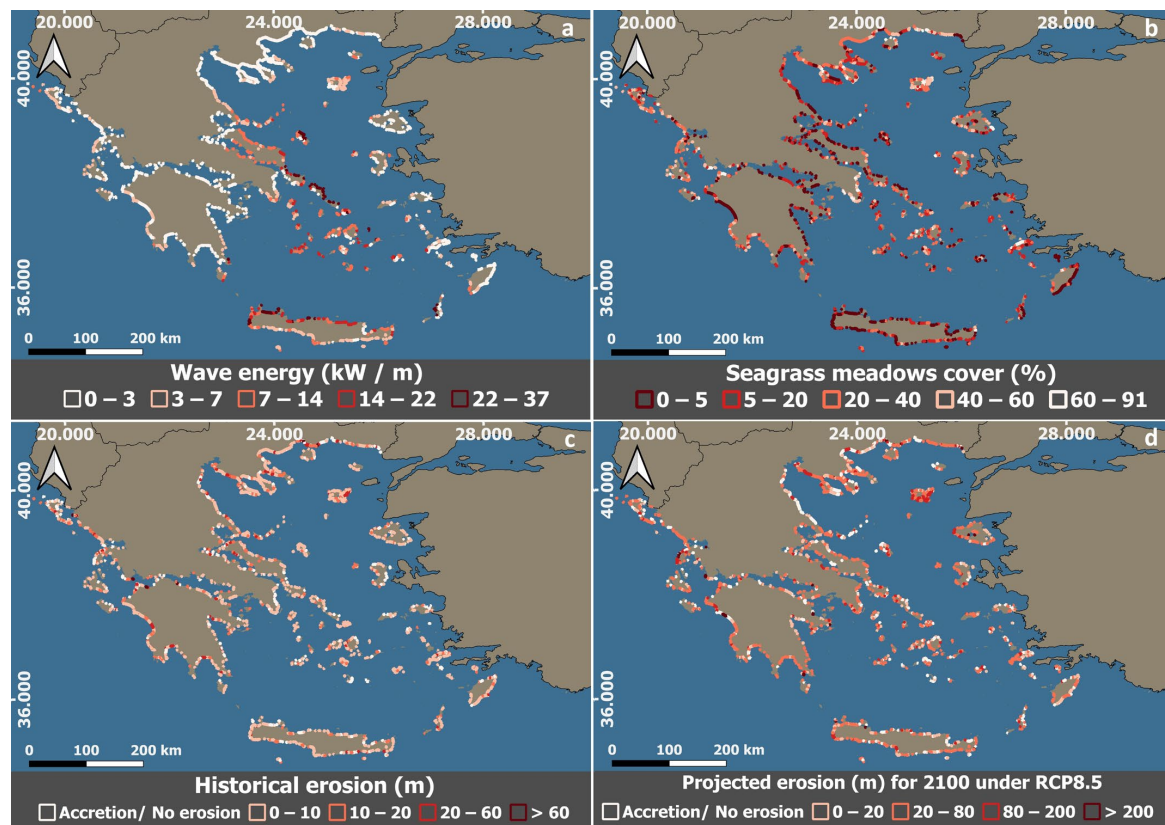


**Figure 2.** Spatial distribution of natural characteristics spatial distribution. (a) Wave energy attributed for each beach in kW/m. (b) Seagrass meadows cover (%) in 1 km radius from each beach. (c) Historical erosion in meters for the period 1984–2015. (d) Projected erosion in meters for the year 2100 under the RCP8.5 climate scenario.

The land-use vulnerability (Figure 3a) also indicates hotspots along the Greek coastline. The highest values (0.73–1) are found across the Chalkidiki peninsulas, where there is dense tourism development along the coast, and Attica that hosts the country’s largest continuous coastal urban footprint. Additional high-vulnerability stretches appear along the northern Peloponnese, parts of northern Crete, and across several island regions including the Cyclades, southeastern Aegean and Ionian islands. These patterns reflect areas where intensive built-up uses, tourism infrastructure and limited coastal space combine to elevate exposure and susceptibility to erosion. The spatial distribution of coastal (hinterland) population (Figure 3b) shows a set of clearly defined demographic hotspots. The highest populations cluster around major urban and tourism areas, most prominently across the Attica coastline, the Chalkidiki peninsulas, and large parts of northern Crete. Additional high-population stretches occur along the Ionian and southeastern Aegean islands and parts of the western Peloponnese. Much of the remaining Greek coastline, including the western mainland and many Aegean islands, is characterized by low to very low populations, reflecting more dispersed settlement structures. Beach recreational use value is highly uneven across Greece, with a small number of internationally renowned destinations concentrating the highest economic activity. The top-value beaches (10–220 million € yr<sup>−1</sup>) are overwhelmingly located in the Cyclades, specifically Mykonos and Santorini, which host the highest individual values in the entire dataset, reaching the upper limit of the mapped range (≈200 million € yr<sup>−1</sup>) (Figure 3c). Comparable high-end values also occur along northern Crete, as well as along the northern coast of Rhodes. Outside these flagship tourism zones, several Ionian island beaches exhibit distinctly elevated values, where concentrated resort development and high seasonal visitation drive substantial demand. Additional high-value

clusters appear central Aegean islands (e.g., Skiathos), and along selected stretches of the Peloponnese, all corresponding to well-developed, high-traffic 3S touristic destinations. In contrast, the majority of mainland and less-developed island coastlines display much lower annual recreational use values, highlighting the strong geographic concentration of Greece's high-value coastal tourism. It is also important to note that beach accessibility is spatially patchy (Figure 3d), and this inequality is reflected in the economic patterns of beach use. Previous research [55] has shown that accessibility provision not only supports equitable coastal use but also strengthens the economic performance of accessible beaches through increased demand and repeat visitation. Wheelchair-user recreational value follows an even more concentrated pattern, with the highest values (1–18 million € yr<sup>-1</sup>) limited to a small number of major tourism and accessibility hubs. The Cyclades remain dominant, with additional notable values along parts of Attica and northern Crete, where both user demand and accessible infrastructure are relatively well developed. The northern coastline of Rhodes forms another smaller hotspot. Most other regions register low to very low values, reflecting the limited and uneven distribution of accessible beach facilities nationwide. Overall, the spatial patterns of natural and socio-economic drivers directly inform the composite indices rather than being interpreted in isolation. High BEI values emerge where energetic wave climates and persistent historical and projected shoreline retreat coincide, unless locally moderated by extensive seagrass cover. SEII hotspots reflect the spatial concentration of land-use intensity, coastal population, tourism-driven recreational value, and accessibility-related benefits. Consequently, the CEVI captures the co-occurrence of physical susceptibility and socio-economic concentration, translating spatial variability into analytically interpretable vulnerability patterns relevant for ICZM prioritization.

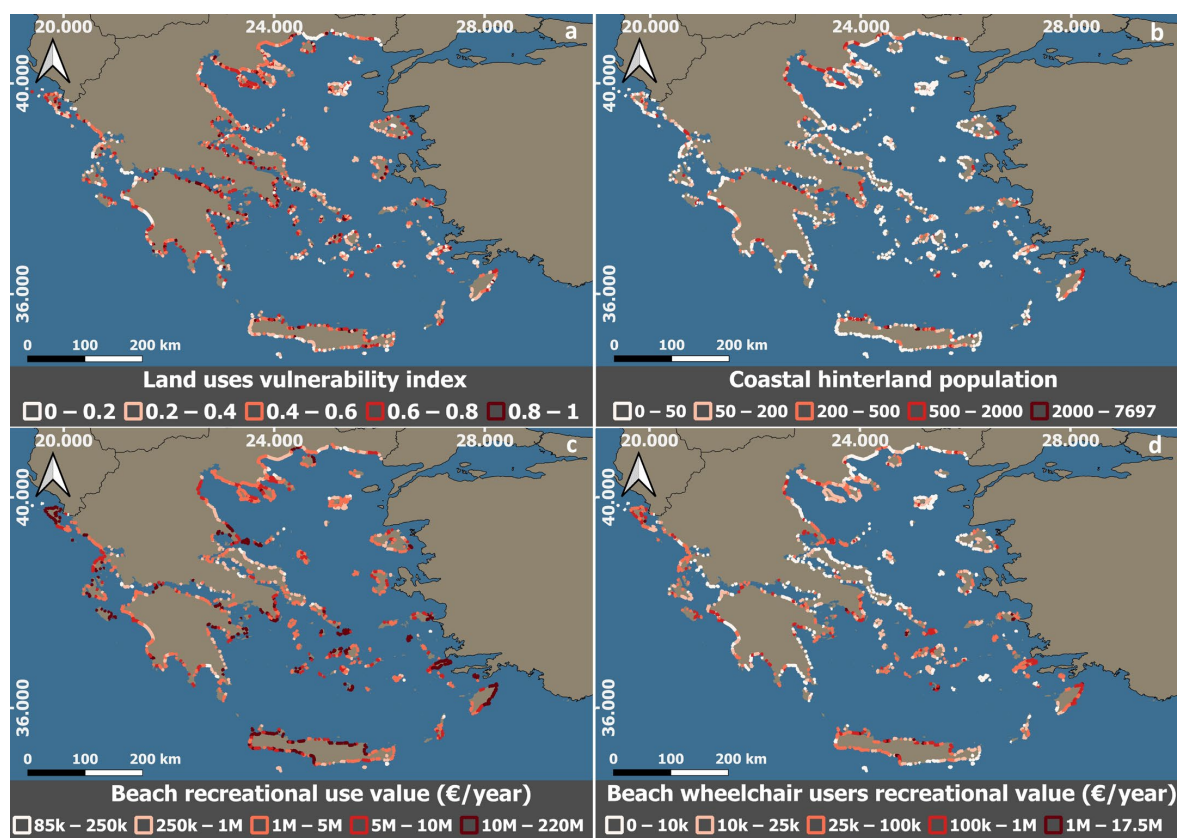


**Figure 3.** Spatial distribution of socio-economic characteristics: (a) Land uses Vulnerability Index spatial distribution; (b) Coastal hinterland population count within 500 m radius from each beach; (c) Beach recreational total use value (€/year/beach), and (d) Beach recreational use value for wheelchair users (€/year/beach).

### 3.2. Coastal Vulnerability: Spatial Distribution

The BEI (Figure 4a) shows a clear concentration of high erodibility values along specific coastal sectors. The highest BEI scores (0.65–1) are overwhelmingly located along northern and southern Crete, forming the most extensive continuous high-risk zone in the country. This pattern aligns with numerous assessments that identify Crete, as one of Greece's most erosion-prone regions due to rapid shoreline retreat, sediment deficits, and intense hydrodynamic forcing [66,67]. A second major hotspot is located around Evia island, where multiple beach segments fall consistently within the highest erodibility class. Chalkidiki exhibits consistently elevated erodibility, with multiple beach segments falling within the 0.51–0.65 range, though not reaching the extreme values observed in Crete. Additional high-risk pockets appear across the Cyclades, the northern and southeastern Aegean islands and the western Peloponnese.

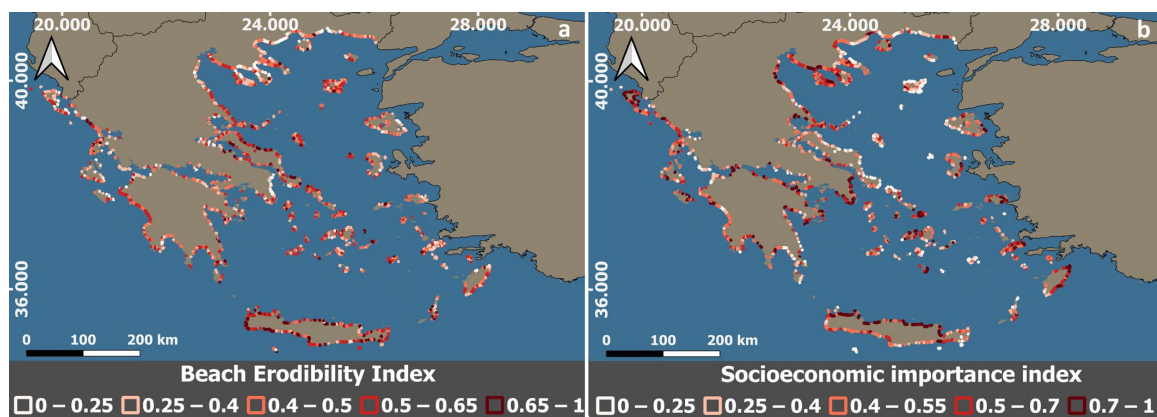


**Figure 4.** (a) Spatial distribution of the Beach Erodibility Index (BEI) and (b) the Socio-Economic Importance Index (SEII) along the Greek coastline. Higher BEI values highlight coastlines characterized by increased geomorphic susceptibility to erosion, while higher SEII values indicate areas with elevated human, economic, and recreational significance.

The spatial distribution of the (SEII) (Figure 4b) highlights several well-defined coastal clusters where socio-economic activity are markedly higher. The highest SEII values (0.72–1) occur along northern, western, and southern Crete, forming the most extensive socio-economic hotspot in the country, consistent with the island's concentration of high-value tourism beaches, large visitor flows, and dense coastal settlements. Comparable high-importance zones are also evident along the Rhodes, Mykonos and Santorini coasts, where intense tourism-driven activity elevates recreational value and coastal population metrics. Additional high-SEII segments appear in Attica, reflecting the combination of large resident populations, and the intensive beach and land-use. Other smaller but distinct high-value clusters are visible in the Cyclades, the central and southeastern Aegean and the Ionian islands. Moderate-to-high SEII values are also present along the northern Aegean coastline.

The Coastal Erosion Vulnerability Index (Figure 5) exhibits a clear concentration of high-vulnerability segments across several well-known erosion-prone coastal areas. The most extensive cluster of very high CEVI values (0.65–1) of all beaches in Greece occurs along northern, northwestern, and southern Crete, forming the single largest continuous zone of elevated erosion in the country. High CEVI values also appear systematically across the Cyclades islands, where exposed island coasts face a combination of energetic wave climate and limited accommodation space [67]. Additional high-vulnerability stretches are visible in Chalkidiki, particularly along the open sea coasts, reflecting both erosive forcing and intense shoreline use. Distinct hotspots are also present in the Ionian and southern



Aegean islands, where exposure to energetic wave conditions combines with significant coastal development pressure. Smaller high-vulnerability pockets are identifiable at the coasts of the other Greek islands. Elevated CEVI values are widespread along the Greek coastline, with over 40% of beaches scoring above 0.5, reflecting broadly heightened erosion-related vulnerability. Within this general pattern, a much smaller set of beaches stands out as persistent, high-intensity hotspots where geomorphic susceptibility and human pressures converge. Close to 5% of beaches exceed a CEVI value of 0.7, forming the most critical zones of erosion vulnerability in the country. Crete, the Cyclades, Chalkidiki, the Ionian and southeastern Aegean islands repeatedly register at the upper end of the index, indicating locations where geomorphic susceptibility and the human–environment development reach their highest levels. These areas therefore represent zones where coastal erosion is not only likely to be more severe but also more consequential for the coastal natural and human environment. Overall, the CEVI spatial pattern reflects the interaction between geomorphic susceptibility (BEI) and socio-economic importance (SEII), rather than a simple amplification of either component alone. Beaches classified in the highest CEVI class (0.65–1), defined using Jenks natural breaks [68], consistently correspond to locations where strong erosive forcing coincides with high concentrations of population, tourism activity, and coastal land use. These upper classes therefore represent statistically distinct clusters within the national vulnerability distribution and are interpreted as relative screening levels that identify priority hotspots for ICZM intervention at national scale, rather than as absolute risk thresholds, supporting comparative prioritization rather than site-specific engineering design.

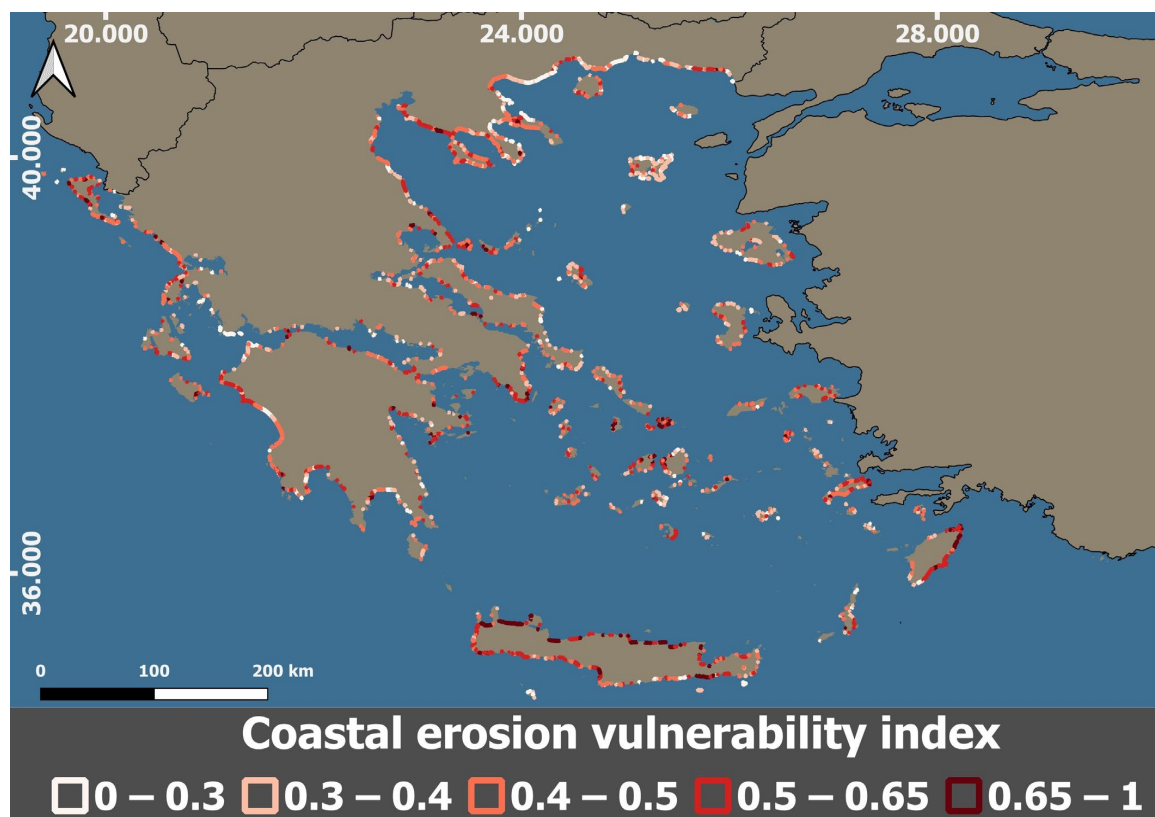


**Figure 5.** Spatial distribution of Coastal Erosion Vulnerability Index (CEVI) for the Greek coastline, classified into five vulnerability classes. Higher values indicate higher vulnerability.



### 3.3. Coastal Flood Exposure Risk: Method Behavior and Spatial Distribution

Coastal flood exposure patterns derived in this study reflect the application of a connectivity-constrained inundation approach, rather than a purely elevation-based static bathtub model. At national scale, traditional bathtub methods tend to substantially overestimate inland flooding by classifying all low-lying areas as inundated, irrespective of their hydraulic connection to the coastline. To address this limitation, the proposed approach restricts flood propagation to inland areas that are topographically and hydraulically connected to the shoreline, yielding more spatially coherent and physically plausible inundation patterns suitable for large-scale screening.

To illustrate the effect of this constraint, two representative coastal sectors are presented in Figure 6. Although shown only for illustrative purposes, these examples are indicative of patterns observed consistently across the study area. In both cases, the static bathtub approach identifies extensive inland flooding (red points), whereas the connectivity-based algorithm substantially reduces false-positive inundation by retaining only hydraulically connected flooded locations (blue points).

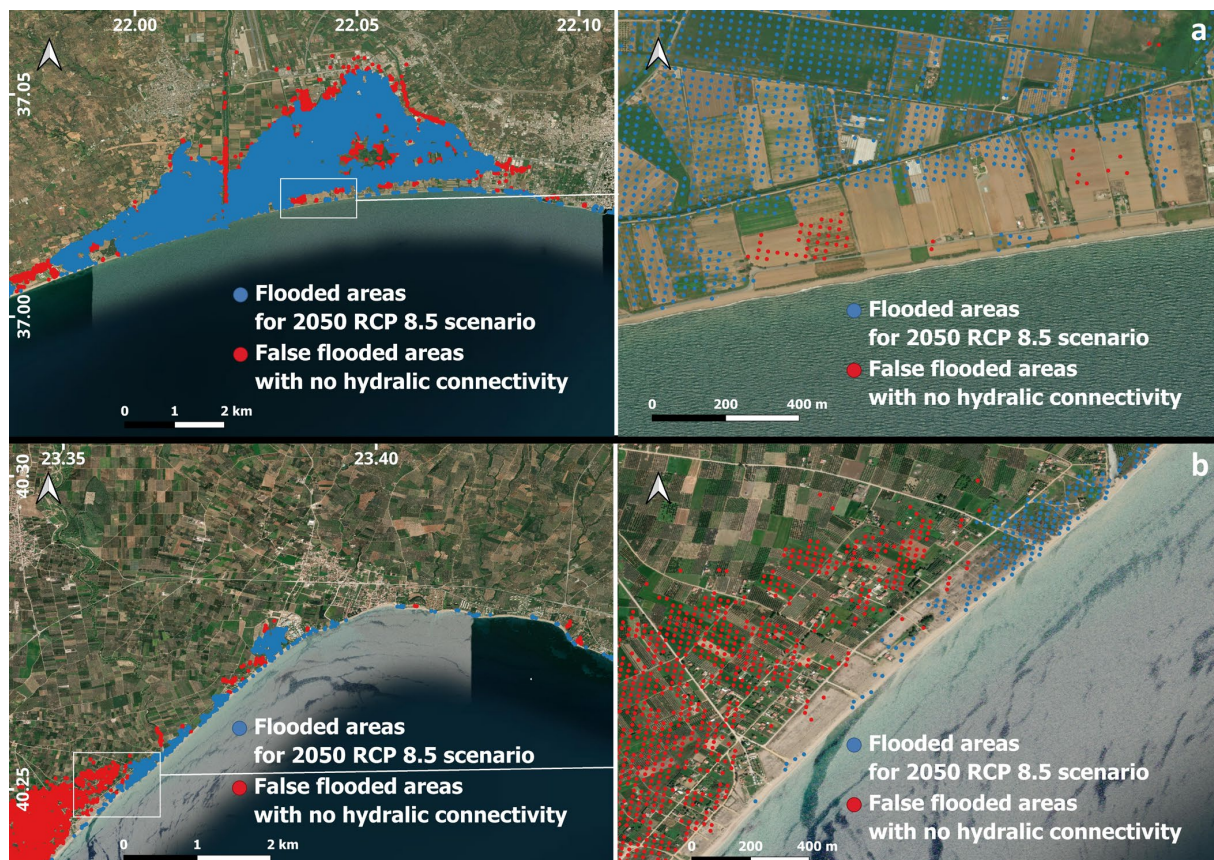


**Figure 6.** Illustration of the connectivity-constrained coastal flood propagation approach under the 2050 RCP 8.5 scenario for two representative coastal sectors in Greece. Blue points indicate flooded locations retained by the hydraulic connectivity algorithm, while red points represent low-elevation locations classified as flooded by a static bathtub approach but excluded due to lack of hydraulic connection to the shoreline. (a) A coastal area west of Kalamata (Southern Peloponnese), characterized by low-lying agricultural land and discontinuous inland connectivity. (b) the coastal sector at Agios Mamas, Chalkidiki (Northern Greece), where the bathtub approach substantially overestimates inland inundation relative to the connectivity-constrained results. Basemap: Esri World Imagery © Esri, Maxar, Earthstar Geographics, and the GIS User Community.

The spatial pattern of the TFEI (Figure 7) under the RCP 8.5 scenario for 2050 reveals extensive low-lying coastal zones with substantial susceptibility to inundation (% of each coastal segment projected to be flooded). Approximately half of the Greek coastline exhibits measurable inundation under the 2050 RCP 8.5 scenario, with about 50% of coastal segments showing at least minor flooding (>1% of their area affected). Flood exposure becomes more pronounced in a smaller subset of locations: around 8% of the coastline experiences inundation exceeding 10%, indicating moderate sensitivity to extreme sea levels. A fraction of segments undergo extensive flooding, with 1.5% of the coastline projected to have more than 50% of its area inundated, representing the most flood-susceptible zones under this scenario. High and very high exposure levels (>50%) are concentrated in several morphodynamically vulnerable deltas, wetlands, and embayments across Greece. In northern Greece, extensive deltaic plains and shallow coastal wetlands exhibit some of the largest inundation footprints, reflecting their low elevations and gentle slopes. Similar patterns occur along parts of the eastern mainland, where semi-enclosed gulfs and coastal plains provide limited natural buffering and allow floodwaters to propagate inland under extreme sea-level conditions. In the northern Aegean islands, high exposure is primarily associated with enclosed bays and inner-gulf environments, where narrow inlets and low-relief shorelines increase susceptibility to inundation. Additional exposed segments are observed along the central mainland, particularly in smaller coastal plains and river-mouth environments with restricted drainage and broad intertidal areas. In western Greece, extensive lagoon complexes and marsh-dominated coasts display consistently high exposure values, while parts of the southern mainland show elevated susceptibility in low-lying bay-head settings. In the Ionian Islands, exposure is concentrated in low-relief coastal stretches with broad nearshore slopes. Overall, the TFEI distribution indicates that flooding susceptibility is highest in deltas, lagoon systems, coastal plains, and bay-head environments, where terrain characteristics combine with projected sea-level rise to produce extensive inundation under RCP 8.5 conditions.

The UFRI (Figure 8) highlights a set of concentrated hotspots where substantial portions of urban fabric fall within the areas projected to be inundated under the RCP 8.5 sea-level rise scenario for 2050. One of the strongest clusters of high urban flood exposure appears along the Thessaloniki metropolitan coastline, including low-lying segments near the international airport and the urban-industrial waterfront extending toward the Axios river mouth. Additional elevated exposure zones occur in eastern Macedonia and Thrace, particularly along major port-adjacent urban frontages where dense development meets low-elevation coastal terrain. In Thessaly, high values are concentrated around the coastal urban area of Volos and nearby low-lying peri-urban zones. In Central Greece, notable hotspots appear in parts of the broader Chalkida urban area and selected adjacent settlements with constrained elevation and limited natural buffering. In Western Greece, extensive high-exposure areas are evident along the Patras metropolitan coastline and surrounding urban corridors. Additional elevated exposure is observed in several medium-sized coastal towns of the western mainland and in selected urbanized parts of the Ionian Islands, where built-up areas are located immediately behind low-relief shorelines. In the northern Aegean, certain port-front urban areas, including those on major islands, also register high exposure levels due to the juxtaposition of dense coastal development and enclosed bay morphology. Collectively, these areas represent the urban segments most sensitive to projected coastal flooding, reflecting the intersection of low-lying development patterns, limited geomorphological protection, and high inundation likelihood under RCP 8.5 conditions.

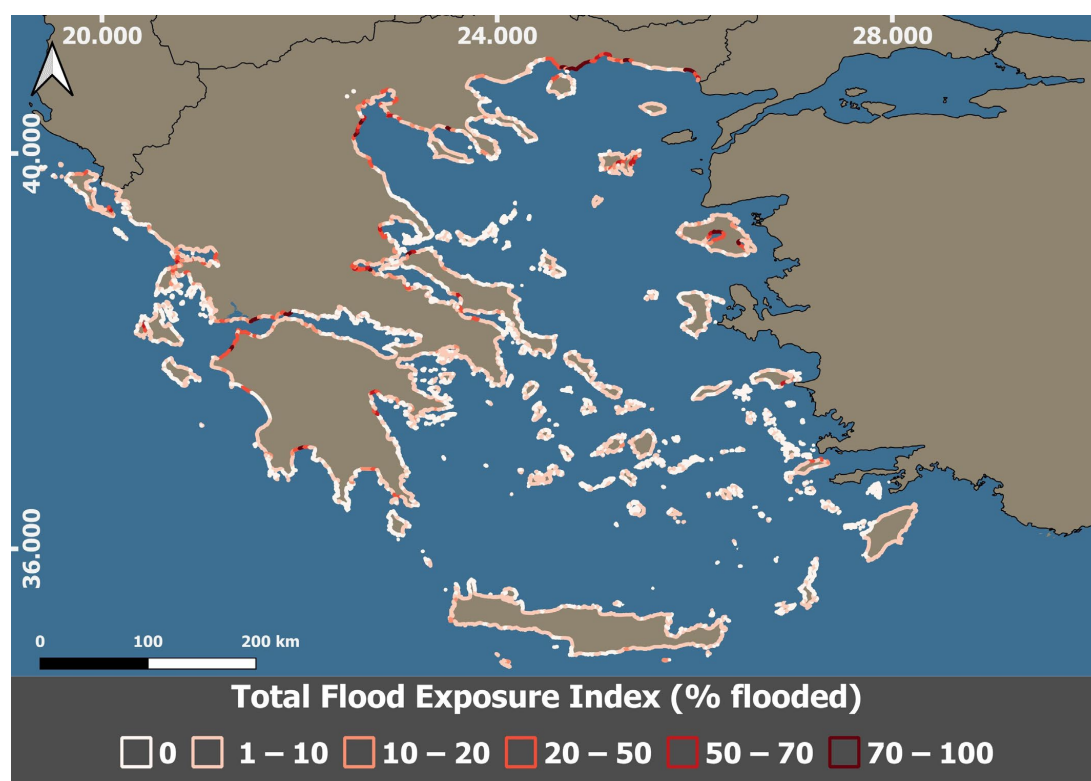


**Figure 7.** Total Flood Exposure Index (TFEI) showing the percentage of each coastal segment projected to be inundated under the RCP 8.5 sea-level rise scenario for 2050 across the Greek coastline.

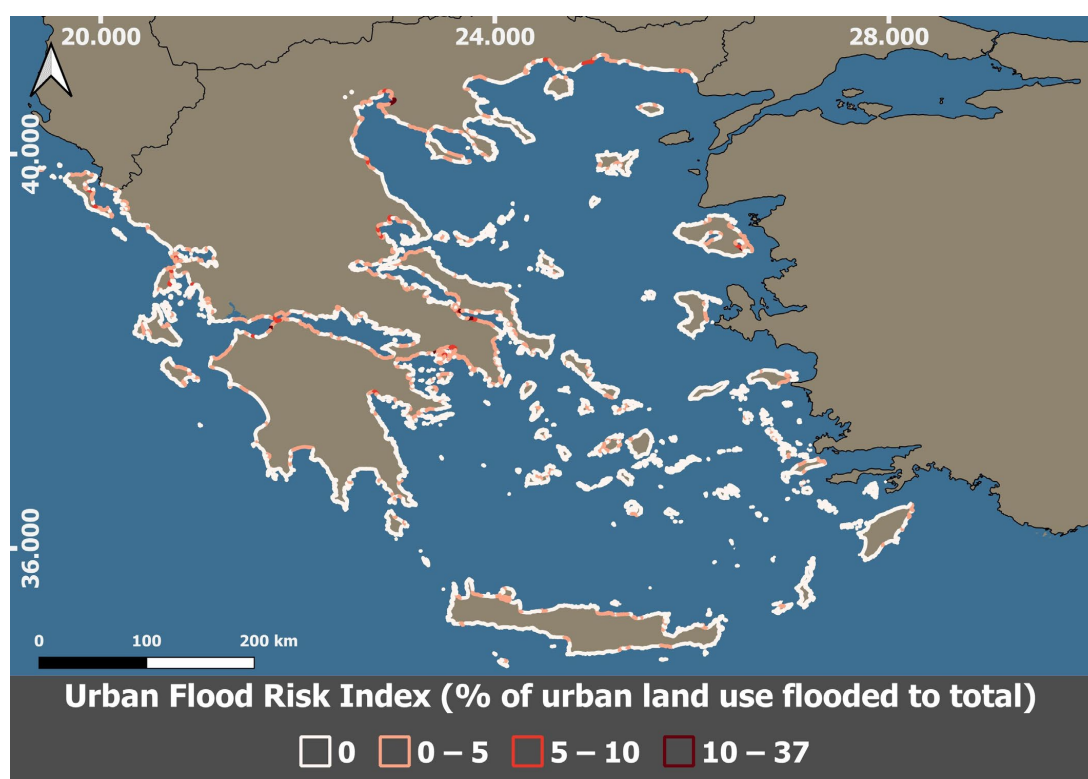


**Figure 8.** Urban Flood Risk Index (UFRI) showing the proportion of urban land projected to be flooded under the RCP 8.5 sea-level rise scenario for 2050.



### 3.4. Indexes Interplay for ICZM

The combined interpretation of erosion- and flood-related indices provides a more nuanced and operational picture of coastal risk than either hazard considered in isolation, which is a core requirement of Integrated Coastal Zone Management (ICZM). The CEVI highlights beaches where chronic, long-term shoreline retreat intersects with high socio-economic and recreational importance, identifying locations where gradual erosion can progressively undermine coastal services, tourism revenue, and accessibility infrastructure. In contrast, the flood exposure indices (TFEI and UFRI) capture episodic but potentially disruptive marine inundation processes acting over broader spatial extents, particularly in low-lying plains, deltas, lagoon systems, and urbanized coastal fronts. The partial spatial overlap between high CEVI and high flood exposure zones indicates that erosion and flooding are often governed by distinct geomorphological and socio-economic controls, reinforcing the need for differentiated management responses rather than a single aggregated risk metric.

From an ICZM perspective, the interplay among indices enables strategic prioritization across multiple adaptation pathways. Coastal sectors characterized by high CEVI but low flood exposure are primarily affected by sediment deficits and wave-driven retreat, suggesting that nature-based solutions, sediment management, and beach-scale interventions may be most effective. Conversely, areas with low erosion vulnerability but high TFEI or UFRI values are dominated by elevation-driven inundation risks, where land-use planning, setback policies, and flood-resilient infrastructure become critical. Locations where high CEVI coincides with high flood exposure represent compound-risk hotspots, where both chronic and extreme hazards threaten coastal systems and human activities simultaneously; these areas warrant integrated, cross-sectoral interventions aligned with ICZM principles. By maintaining separate but complementary indices within a unified geospatial framework, the approach supports transparent screening, comparison, and decision-making across governance levels, without obscuring hazard-specific dynamics that are essential for effective coastal adaptation planning.

## 4. Discussion

This study develops a reproducible, open-access geospatial framework for ICZM under climate change, designed to support large-scale vulnerability assessment and adaptation planning. The framework integrates harmonized European datasets, multi-criteria coastal-erosion indicators, and an automated flood-propagation model, offering a scalable approach that can be transferred to other coastal regions. Greece serves as the pilot application for testing and demonstrating the methodology, revealing how the combined erosion–flood assessment can highlight spatial patterns of physical susceptibility, socio-economic exposure, and priority adaptation needs.

Several methodological choices reflect deliberate trade-offs required for national-scale screening. Proximity-based assignment of offshore wave conditions and shoreline-change values to beach polygons assumes that the nearest available observations provide a reasonable proxy for local forcing. While this approach ensures spatial consistency and computational efficiency across the entire coastline, it does not resolve fine-scale processes such as nearshore wave transformation, local bathymetric effects, or alongshore sediment connectivity that influence site-specific erosion dynamics. Similarly, the use of fixed buffer distances to represent nearshore and backshore influence zones reflects a pragmatic standardization choice. In reality, the spatial extent over which a given variable (e.g., population exposure, land use, or seagrass influence) affects beach vulnerability can differ substantially among beaches due to variations in slope, morphology, and coastal configuration. Applying a single buffer distance therefore cannot capture these site-specific differences; however,

introducing variable, beach-specific buffers would require detailed local information and assumptions that are not feasible or defensible at national scale. The adopted buffers thus support consistent comparison and screening, while acknowledging that locally tailored buffer extents would be necessary for detailed, site-scale applications. In addition, the erosion component focuses on shoreline retreat by treating stable or accreting conditions as neutral, prioritizing vulnerability screening over full representation of shoreline-change dynamics. While these simplifications may limit local-scale precision, they ensure spatial consistency, reproducibility, and interpretability across the entire coastline and are appropriate for comparative, first-order assessment within an ICZM-oriented national framework.

The robustness of the framework is supported by the maturity and reliability of the underlying datasets and methods. For the erosion component, all input variables, including historical shoreline change, projected shoreline retreat, offshore wave energy, and seagrass meadow cover, are drawn from well-established, peer-reviewed products that have undergone extensive use and validation in global, European, and national studies [38–40,69,70]. Their repeated application in large-scale coastal assessments provides an indirect but meaningful level of confidence for their use in this study. In our results, the spatial patterns produced by these datasets also correspond closely with well-documented erosion hotspots in Greece, as reported in regional studies cited in Section 3. This agreement further supports the plausibility of the derived indices without requiring additional site-specific validation at this national-scale screening level. For the flooding component, the analytical aim is national-level susceptibility screening rather than detailed hydrodynamic simulation. As such, the flood exposure results are not validated against site-specific empirical inundation observations, but are intended as first-order indicators of relative susceptibility suitable for national-scale screening and prioritization. Under this objective, formal validation using event-based inundation observations is not essential, particularly given the absence of consistent, country-wide validation datasets. The propagation-based method used here improves upon static bathtub approaches by enforcing topographic connectivity, and the resulting inundation patterns align well with geomorphologically expected high-risk areas, including deltas, lagoon systems, bay-head environments, and low-lying coastal urban zones. Future work may incorporate calibrated 2D hydrodynamic models in priority areas to support local-scale validation and more refined adaptation planning.

Across Greece, natural and socio-economic indicators reveal a strongly uneven distribution of coastal pressures and values. Wave energy is highest along exposed island and open-coast sectors, while seagrass cover and historical shoreline retreat highlight recurrent erosion-prone regions such as Crete, Chalkidiki, and parts of the northern Aegean; these patterns persist under projected shoreline retreat, indicating sustained geomorphological susceptibility. Socio-economic characteristics show similar concentration, with high land-use vulnerability, dense coastal populations, and the highest recreational beach-use values occurring in major tourism zones, while accessibility remains spatially uneven, producing a highly localized distribution of wheelchair-user use value. CEVI is highest where physical susceptibility aligns with concentrated human use, particularly in Crete, the Cyclades, Chalkidiki, and parts of the Ionian and southeastern Aegean islands. Flood exposure represents an independent assessment based on the inundation modeling framework and highlights extensive susceptibility in low-lying deltas, lagoon systems, bay-head environments, and major coastal urban centers, where the topographic conditions allow substantial inland propagation of extreme sea levels. Together, they identify priority regions where different hazards and pressures converge and where targeted, hazard-specific measures within an integrated ICZM framework are most urgently needed.

A central component of the methodology is the use of the CLC Coastal Zones 2018 dataset of the Copernicus Land Monitoring Service, using the beach polygons delineated



in this dataset as the spatial foundation for the erosion-vulnerability analysis. To evaluate the representativeness of the beach layers, the polygons for the Aegean Archipelago were compared with those mapped by Monioudi et al., 2017 [67]. The comparison indicated that the Copernicus dataset contains approximately one-third of the beach polygons identified in the earlier manual mapping; however, the total mapped beach area is broadly comparable. This difference primarily reflects methodological distinctions: the automated Copernicus delineation occasionally merges long coastal stretches into single beach polygons and omits very small pocket beaches that fall below its minimum mapping threshold, whereas the manual mapping applied finer segmentation into smaller, discrete units. Similar limitations of the CLC Coastal Zones 2018 product have been previously acknowledged in its application within the pan-European Early Warning and Coastal Monitoring System [71], where small-scale morphological features were sometimes underrepresented. As a result, very small pocket beaches may be underrepresented in the present analysis, which can limit applicability at fine local scales and may lead to underestimation of vulnerability in highly localized settings. Nonetheless, both the present comparison and previous European-scale evaluations confirm that, despite its coarser segmentation, the Copernicus dataset provides a highly reliable and harmonized depiction of coastal morphology, well suited for reproducible, large-scale, and national-level vulnerability assessments.

Another practical methodological decision in the framework is the use of RCP-based climate projections instead of SSP-based scenarios [64]. This choice reflects the current state of available open-access European impact datasets: key inputs such as JRC Extreme Sea Level projections and shoreline-change models are released only under the RCP framework. Equivalent SSP-based geospatial datasets have not yet been published in operational, harmonized form. The use of RCPs therefore ensures consistency, compatibility, and reproducibility across the full modeling chain. While this choice reflects current data availability rather than a conceptual preference, it does not limit the long-term applicability of the framework. As harmonized SSP-based coastal impact datasets become available, the methodology can be directly updated, and future extensions may incorporate site-specific hydrodynamic validation, infrastructure-focused exposure layers, and temporally resolved population dynamics to support more detailed local-scale applications.

This study represents the first national-scale assessment of coastal flood risk in Greece that integrates high-resolution land data with hydrodynamic projections, offering a reproducible framework for large-scale adaptation planning. Future research could build upon these findings, by considering also the evolving regulation [72] and incorporating spatially explicit information on critical infrastructure, as prescribed in the EU Directive 2022/2557 [73] on the resilience of critical entities, to better align coastal-risk assessments with civil protection and resilience planning. Further refinement is also needed to assess exposure across protected natural areas (e.g., Natura 2000 sites) and zones of high population density, particularly in regions experiencing pronounced seasonal population increases during the summer months. Integrating these dimensions would enhance the framework's capacity to guide targeted, cross-sectoral adaptation actions that address both environmental and socio-economic vulnerabilities along the coast.

Despite the implicit inclusion of geological and anthropogenic influences in the ambient shoreline-change component, the framework does not independently resolve spatially variable vertical land motions which can have a major role when estimating future relative sea-level rise along the coast [74,75]. While recent datasets such as the Copernicus European Ground Motion Service (EGMS) provide high-resolution time series of land subsidence and uplift across Europe [76], their integration was beyond the scope of this screening-level assessment. The adopted approach prioritizes methodological consistency and parsimony, while acknowledging that future developments could couple erosion projections with

explicit vertical land-motion data to refine relative sea-level rise estimates and improve site-specific coastal vulnerability assessments.

In the present study, coastal flooding and erosion projections are based on global probabilistic modeling frameworks [61] where projection of SLR in the Mediterranean Sea are driven by the Atlantic forcing on Gibraltar derived from downscaled global outputs. Mediterranean Sea is a marginal basin whose complex, basin scale atmospheric and oceanographic processes have been noted to not be fully resolved by Global Climate Model projections [77]. Therefore, while the applied erosion and ESL projections provide internally consistent and widely validated datasets suitable for first-order, national-scale assessments the adoption of Mediterranean-focused sea-level rise and extreme sea-level datasets [78] is strongly encouraged in future applications of the proposed framework, as they would allow a more accurate representation of regional oceanographic processes and further improve coastal vulnerability assessments at sub-national and local scales.

## 5. Conclusions

Overall, the work presents a transferable, climate-ready geospatial framework that operationalizes ICZM principles using fully open-access datasets. By combining scalable erosion and flood assessment methods within a unified structure, the framework provides a first-order, screening-level tool for identifying priority areas, guiding resource allocation, and supporting long-term adaptation pathways under accelerating coastal change.

The results from the Greek pilot illustrate the framework's ability to identify recurrent high-vulnerability beach clusters where geomorphological constraints and intense human use intersect with climate-driven hazards. By integrating biophysical attributes (e.g., shoreline change, wave energy, seagrass presence) with socio-economic and accessibility parameters, the framework expands beyond traditional CVI-type approaches and reflects the multifunctional nature of beaches as socio-ecological systems. This supports ICZM principles by encouraging the joint consideration of environmental processes and human use, while remaining index-based and semi-quantitative in nature. For coastal flooding, the propagation-based inundation approach provides a more spatially constrained representation of exposure by accounting for topographic connectivity, reducing the overestimation typical of static planar "bathtub" models [56]. The resulting patterns are consistent with geomorphologically susceptible settings such as deltaic plains, lagoon systems, enclosed embayments, and low-lying urban coastal zones. These results support spatially explicit identification and comparison of flood-exposed coastal zones at national scale, providing a robust basis for prioritization and strategic adaptation planning, while recognizing that site-specific forecasting would require locally calibrated hydrodynamic models.

While the framework is fully operational for national-scale screening using currently available datasets, its scalability and transferability are contingent on the availability of comparable, harmonized geospatial inputs. Extension to finer-scale applications or process-resolving assessments will require additional developments, including SSP-based extreme sea-level projections, integration of critical infrastructure and ecosystem datasets, and local-scale hydrodynamic validation in priority areas. These developments are necessary to expand the scope and resolution of the framework, while preserving its current function as a robust, reproducible tool for strategic coastal risk screening and ICZM-oriented planning under ongoing climate change. The proposed framework is not intended to replace local knowledge, post-disaster decision-making, or the economic and political considerations that shape coastal management in practice. Instead, it is designed as a pre-disaster, national-scale screening tool to support planners and technical authorities in identifying and comparing areas where erosion and flooding pressures are likely to be most pronounced. By relying on harmonized, open-access datasets and transparent geospatial

workflows, the framework is readily applicable across large and heterogeneous coastlines and supports strategic prioritization and anticipatory planning, while complementing, rather than replacing, local-scale assessments and decision processes.

**Author Contributions:** Conceptualization, T.C., D.C. and A.F.V. Data curation, T.C., D.C., V.S. and I.N.M. Formal analysis, T.C., D.C. and V.S. Methodology, T.C., D.C., V.S., I.N.M., S.K. and A.F.V., Supervision A.F.V. and S.K. Visualization, T.C., Writing—original draft, T.C., D.C. and V.S. Writing—review and editing, T.C., D.C., V.S., I.N.M., S.K. and A.F.V. All authors have read and agreed to the published version of the manuscript.

**Funding:** V.S. and S.K. were supported by the European Union’s Horizon 2020 research and innovation program HORIZON-CL6–2021-BIODIV-01–04 under grant agreement No. 101059877 “GES4SEAS—Achieving Good Environmental Status for maintaining ecosystem Services, by Assessing integrated impacts of cumulative pressures” and by Biodiversa+, the European Biodiversity Partnership, in the context of the INSPIRE project under the 2021–2022 BiodivProtect joint call. It was co-funded by the European Commission (GA No. 101052342) and the following funding organizations: Agencia Estatal de Investigación (Spain), Ministero dell’Università e della Ricerca (Italy), Swiss National Science Foundation (Switzerland), Fundação para a Ciência e a Tecnologia (Portugal), Der Wissenschaftsfonds (Austria), General Secretariat for Research and Innovation (Greece) and Salford University (UK).

**Data Availability Statement:** The data presented in this study are openly available in Integrated-Coastal-Zone-Management-Framework-for-Greece at <https://github.com/Airenus/Integrated-Coastal-Zone-Management-Framework-for-Greece> (accessed on 11 January 2026).

**Conflicts of Interest:** The authors declare no conflicts of interest.

## Abbreviations

The following abbreviations are used in this manuscript:

ICZM	Integrated Coastal Zone Management
CVI	Coastal Vulnerability Index
CEVI	Coastal Erosion Vulnerability Index
BEI	Beach Erodibility Index
SEII	Socio-Economic Importance Index
TFEI	Total Flood Exposure Index
UFRI	Urban Flood Risk Index
DEM	Digital Elevation Model
ESL	Extreme Sea Level
RCP	Representative Concentration Pathway
SSP	Shared Socioeconomic Pathway
CMEMS	Copernicus Marine Environment Monitoring Service
CLMS	Copernicus Land Monitoring Service
CLC	CORINE Land Cover
JRC	Joint Research Centre (European Commission)
GHSL	Global Human Settlement Layer
TOPSIS	Technique for Order of Preference by Similarity to Ideal Solution
WGS 84	World Geodetic System 1984

## References

1. Armstrong McKay, D.I.; Staal, A.; Abrams, J.F.; Winkelmann, R.; Sakschewski, B.; Loriani, S.; Fetzer, I.; Cornell, S.E.; Rockström, J.; Lenton, T.M. Exceeding 1.5 °C global warming could trigger multiple climate tipping points. *Science* **2022**, *377*, eabn7950. [CrossRef]
2. Lenton, T.M.; Milkoreit, M.; Willcock, S.; Abrams, J.F.; Armstrong McKay, D.I.; Buxton, J.E.; Donges, J.F.; Loriani, S.; Wunderling, N.; Alkemade, F.; et al. (Eds.) *The Global Tipping Points Report 2025*; University of Exeter: Exeter, UK, 2025.

3. Cheng, L.; von Schuckmann, K.; Abraham, J.P.; Trenberth, K.E.; Mann, M.E.; Zanna, L.; England, M.H.; Zika, J.D.; Fasullo, J.T.; Yu, Y.; et al. Past and future ocean warming. *Nat. Rev. Earth Environ.* **2022**, *3*, 776–794; Correction in *Nat. Commun.* **2024**, *15*, 9131. [\[CrossRef\]](#)
4. Alter, K.; Jacquemont, J.; Claudet, J.; Lattuca, M.E.; Barrantes, M.E.; Marras, S.; Manríquez, P.H.; González, C.P.; Fernández, D.A.; Peck, M.A.; et al. Hidden impacts of ocean warming and acidification on biological responses of marine animals revealed through meta-analysis. *Nat. Commun.* **2024**, *15*, 2885. [\[CrossRef\]](#) [\[PubMed\]](#)
5. Wu, Y.; Zheng, Z.; Chen, X.; Zhong, W.; Yuan, X.; Zhong, W.; Lei, R.; Li, C.; Zhuang, Y.; Gao, X.; et al. Amplified warming accelerates deoxygenation in the Arctic Ocean. *Nat. Clim. Change* **2025**, *15*, 859–865. [\[CrossRef\]](#)
6. Nikolaou, A.; Katsanevakis, S. Marine extinctions and their drivers. *Reg. Environ. Change* **2023**, *23*, 88. [\[CrossRef\]](#)
7. Wernberg, T.; Thomsen, M.S.; Baum, J.K.; Bishop, M.J.; Bruno, J.F.; Coleman, M.A.; Filbee-Dexter, K.; Gagnon, K.; He, Q.; Murdiyarso, D.; et al. Impacts of climate change on marine foundation species. *Annu. Rev. Mar. Sci.* **2024**, *16*, 247–282. [\[CrossRef\]](#)
8. Garrabou, J.; Gómez-Gras, D.; Medrano, A.; Cerrano, C.; Ponti, M.; Schlegel, R.; Bensoussan, N.; Turicchia, E.; Sini, M.; Gerovasileiou, V.; et al. Marine heatwaves drive recurrent mass mortalities in the Mediterranean Sea. *Glob. Change Biol.* **2022**, *28*, 5708–5725. [\[CrossRef\]](#)
9. Grant, L.; Vanderkelen, I.; Gudmundsson, L.; Fischer, E.; Seneviratne, S.I.; Thiery, W. Global emergence of unprecedented lifetime exposure to climate extremes. *Nature* **2025**, *641*, 374–379. [\[CrossRef\]](#) [\[PubMed\]](#)
10. Hanley, M.E.; Bouma, T.J.; Mossman, H.L. The gathering storm: Optimizing management of coastal ecosystems in the face of a climate-driven threat. *Ann. Bot.* **2020**, *125*, 197–212. [\[CrossRef\]](#)
11. Griggs, G.; Reguero, B.G.; Griggs, G.; Reguero, B.G. Coastal Adaptation to Climate Change and Sea-Level Rise. *Water* **2021**, *13*, 2151. [\[CrossRef\]](#)
12. Monioudi, I.N.; Vousdoukas, M.I.; Giardino, A.; Stocchino, A.; Mentaschi, L.; Feyen, L. Impacts of sea level rise and adaptation across Asia and the Pacific. *Sci. Rep.* **2025**, *15*, 35742. [\[CrossRef\]](#) [\[PubMed\]](#)
13. Rizzetto, F. Effects of Climate Change on the Morphological Stability of the Mediterranean Coasts: Consequences for Tourism. In *Climate Change, Hazards and Adaptation Options, Climate Change Management*; Leal Filho, W., Nagy, G.J., Borga, M., Chávez Muñoz, P.D., Magnuszewski, A., Eds.; Springer International Publishing: Cham, Switzerland, 2020; pp. 761–775. [\[CrossRef\]](#)
14. Karditsa, A.; Niavis, S.; Paramana, T.; Monioudi, I.; Poulos, S.; Hatzaki, M. Is the insular coastal tourism of western Greece at risk due to climate induced sea level rise? *Ocean Coast. Manag.* **2024**, *251*, 107088. [\[CrossRef\]](#)
15. Cruz-Ramírez, C.J.; Chávez, V.; Silva, R.; Muñoz-Perez, J.J.; Rivera-Arriaga, E. Coastal Management: A Review of Key Elements for Vulnerability Assessment. *J. Mar. Sci. Eng.* **2024**, *12*, 386. [\[CrossRef\]](#)
16. Gornitz, V. Global coastal hazards from future sea level rise. *Palaeogeogr. Palaeoclimatol. Palaeoecol.* **1991**, *89*, 379–398. [\[CrossRef\]](#)
17. Thieler, E.R.; Hammar-Klose, E.S. *National Assessment of Coastal Vulnerability to Sea-Level Rise: Preliminary Results for the U.S. Gulf of Mexico Coast*; (No. 2000–179), Open-File Report; U.S. Geological Survey: Reston, VA, USA, 2000. [\[CrossRef\]](#)
18. Monioudi, I.; Chatzistratis, D.; Chalazas, T.; Chatzipavlis, A.; Velegrakis, A.; Andreadis, O.; Monioudis, E.; Nikolaou, A.; Hasiotis, T. A Prioritization Framework for Adaptation Responses for Climate Change-Induced Erosion in Island Beaches—Cases from the Aegean Islands, Greece. *J. Mar. Sci. Eng.* **2025**, *13*, 491. [\[CrossRef\]](#)
19. Chalazas, T.; Bove, G.; Chatzistratis, D.; Monioudi, I.N.; Velegrakis, A.F. A system for the management of sandy shorelines under climate change: United States Virgin Islands (USVI). *Ambio* **2024**, *53*, 406–420. [\[CrossRef\]](#) [\[PubMed\]](#)
20. Manno, G.; Azzara, G.; Lo Re, C.; Martinello, C.; Basile, M.; Rotigliano, E.; Ciraolo, G. An Approach for the Validation of a Coastal Erosion Vulnerability Index: An Application in Sicily. *J. Mar. Sci. Eng.* **2023**, *11*, 23. [\[CrossRef\]](#)
21. Tanim, A.H.; Goharian, E.; Moradkhani, H. Integrated socio-environmental vulnerability assessment of coastal hazards using data-driven and multi-criteria analysis approaches. *Sci. Rep.* **2022**, *12*, 11625. [\[CrossRef\]](#)
22. Bukvic, A.; Rohat, G.; Apotsos, A.; de Sherbinin, A. A Systematic Review of Coastal Vulnerability Mapping. *Sustainability* **2020**, *12*, 2822. [\[CrossRef\]](#)
23. Gasalla-López, B.; Arcila-Garrido, M.; Chica-Ruiz, J.A. Assessment of Climate Vulnerability Indices for Coastal Tourism Destinations. *Atmosphere* **2025**, *16*, 1171. [\[CrossRef\]](#)
24. Velegrakis, A.F.; Chatzistratis, D.; Chalazas, T.; Armaroli, C.; Schiavon, E.; Alves, B.; Grigoriadis, D.; Hasiotis, T.; Ieronymidi, E. Earth observation technologies, policies and legislation for the coastal flood risk assessment and management: A European perspective. *Anthr. Coasts* **2024**, *7*, 3. [\[CrossRef\]](#)
25. Copernicus Marine Service. Copernicus Marine Environment Monitoring Service (CMEMS). European Union. 2025. Available online: <https://marine.copernicus.eu/access-data/> (accessed on 11 January 2026).
26. Copernicus Land Monitoring Service. Copernicus Land Monitoring Service (CLMS). European Union. 2025. Available online: <https://land.copernicus.eu/en/dataset-catalog> (accessed on 11 January 2026).
27. JRC (Joint Research Centre). JRC Data & Services Portal. European Commission. 2025. Available online: <https://data.jrc.ec.europa.eu/> (accessed on 28 November 2025).



28. Andreoli, E.; Brossard, J.; Castellani, C.; Guennal, L.; Kyriazi, Z.; O'Hagan, A.M.; Sciacca, G.; Jacob, C.; Laroussinie, O. *Baseline Assessment on National and Regional Implementation of MSP and Gap Analysis*; REGINA-MSP Project; European Climate, Infrastructure and Environment Executive Agency: Brussels, Belgium, 2024.
29. Petrakis, S.; Karditsa, A.; Alexandrakakis, G.; Monioudi, I.; Andreadis, O. Coastal erosion: Causes and examples from Greece. In *Proceedings of the Coastal Landscapes, Mining Activities & Preservation of Cultural Heritage*, Milos Island, Greece, 17–20 September 2014.
30. Velegrakis, A.F.; Monioudi, I.; Tzoraki, O.; Vousdoukas, M.I.; Tragou, E.; Hasiotis, T.; Asariotis, R.; Andreadis, O. Coastal Hazards and Related Impacts in Greece. In *The Geography of Greece: Managing Crises and Building Resilience*; Darques, R., Sidiropoulos, G., Kalabokidis, K., Eds.; Springer International Publishing: Cham, Switzerland, 2024; pp. 353–370. [\[CrossRef\]](#)
31. European Environment Agency—Copernicus Land Monitoring Service. Coastal Zones Land Cover/Land Use 2018 (Vector), Europe, 6-Yearly. 2020. Available online: <https://land.copernicus.eu/en/products/coastal-zones> (accessed on 28 November 2025).
32. European Commission. Recommendation of the European Parliament and of the Council of 30 May 2002 Concerning the Implementation of Integrated Coastal Zone Management in Europe (2002/413/EC). Official Journal of the European Communities, L148/24. 2002. Available online: <https://eur-lex.europa.eu/legal-content/EN/TXT/?uri=CELEX%3A32002H0413> (accessed on 11 January 2026).
33. European Commission. Directive 2008/56/EC of the European Parliament and of the Council of 17 June 2008 Establishing a Framework for Community Action in the Field of Marine Environmental Policy (Marine Strategy Framework Directive). Official Journal of the European Union, L164/19. 2008. Available online: <https://eur-lex.europa.eu/eli/dir/2008/56/oj> (accessed on 11 January 2026).
34. Korres, G.; Ravdas, M.; Zacharioudaki, A.; Denaxa, D.; Sotiropoulou, M. Mediterranean Sea Waves Reanalysis (CMEMS Med-Waves, MedWAM3 System) (Version 1) (Dataset). Copernicus Monitoring Environment Marine Service (CMEMS). 2021. Available online: [https://data.marine.copernicus.eu/product/MEDSEA\\_MULTIYEAR\\_WAV\\_006\\_012/description](https://data.marine.copernicus.eu/product/MEDSEA_MULTIYEAR_WAV_006_012/description) (accessed on 28 November 2025).
35. Wright, L.D.; Short, A.D. Morphodynamic variability of surf zones and beaches: A synthesis. *Mar. Geol.* **1984**, *56*, 93–118. [\[CrossRef\]](#)
36. Mentaschi, L.; Vousdoukas, M.; Pekel, J.F.; Voukouvalas, E.; Feyen, L. Global Long-Term Shoreline Evolution. European Commission, Joint Research Centre (JRC) (Dataset). 2018. Available online: <http://data.europa.eu/89h/944f6d9b-2fbf-422e-ae3e-4b3aa391ed48> (accessed on 11 January 2026).
37. Vousdoukas, M.I.; Ranasinghe, R.; Mentaschi, L.; Plomaritis, T.A.; Athanasiou, P.; Luijendijk, A.; Feyen, L. Sandy coastlines under threat of erosion. *Nat. Clim. Change* **2020**, *10*, 260–263. [\[CrossRef\]](#)
38. Tierolf, L.; Haer, T.; Athanasiou, P.; Luijendijk, A.P.; Botzen, W.J.W.; Aerts, J.C.J.H. Coastal adaptation and migration dynamics under future shoreline changes. *Sci. Total Environ.* **2024**, *917*, 170239. [\[CrossRef\]](#)
39. Athanasiou, P.; van Dongeren, A.; Giardino, A.; Vousdoukas, M.I.; Ranasinghe, R.; Kwadijk, J. Uncertainties in projections of sandy beach erosion due to sea level rise: An analysis at the European scale. *Sci. Rep.* **2020**, *10*, 11895. [\[CrossRef\]](#) [\[PubMed\]](#)
40. Athanasiou, P.; van Dongeren, A.; Pronk, M.; Giardino, A.; Vousdoukas, M.; Ranasinghe, R. Global Coastal Characteristics (GCC): A global dataset of geophysical, hydrodynamic, and socioeconomic coastal indicators. *Earth Syst. Sci. Data* **2024**, *16*, 3433–3452. [\[CrossRef\]](#)
41. Panayotidis, P.; Papathanasiou, V.; Gerakaris, V.; Fakiris, E.; Orfanidis, S.; Papatheodorou, G.; Kosmidou, M.; Georgiou, N.; Drakopoulou, V.; Loukaidi, V. Seagrass Meadows in The Greek Seas. *SEANOE* **2022**. [\[CrossRef\]](#)
42. Panayotidis, P.; Papathanasiou, V.; Gerakaris, V.; Fakiris, E.; Orfanidis, S.; Papatheodorou, G.; Kosmidou, M.; Georgiou, N.; Drakopoulou, V.; Loukaidi, V. Seagrass meadows in the Greek Seas: Presence, abundance and spatial distribution. *Bot. Mar.* **2022**, *65*, 289–299. [\[CrossRef\]](#)
43. Manca, E.; Cáceres, I.; Alsina, J.M.; Stratigaki, V.; Townend, I.; Amos, C.L. Wave energy and wave-induced flow reduction by full-scale model *Posidonia oceanica* seagrass. *Cont. Shelf Res.* **2012**, *50–51*, 100–116. [\[CrossRef\]](#)
44. Telesca, L.; Belluscio, A.; Criscoli, A.; Ardizzone, G.; Apostolaki, E.T.; Frascchetti, S.; Gristina, M.; Knittweis, L.; Martin, C.S.; Pergent, G.; et al. Seagrass meadows (*Posidonia oceanica*) distribution and trajectories of change. *Sci. Rep.* **2015**, *5*, 12505. [\[CrossRef\]](#)
45. Athanasiou, P.; van Dongeren, A.; Giardino, A.; Vousdoukas, M.; Gaytan-Aguilar, S.; Ranasinghe, R. Global distribution of nearshore slopes with implications for coastal retreat. *Earth Syst. Sci. Data* **2019**, *11*, 1515–1529. [\[CrossRef\]](#)
46. Gacia, E.; Duarte, C.M. Sediment Retention by a Mediterranean Meadow: The Balance between Deposition and Resuspension. *Estuar. Coast. Shelf Sci.* **2001**, *52*, 505–514. [\[CrossRef\]](#)
47. Peduzzi, P.; Velegrakis, A.; Chatenoux, B.; Estrella, M.; Karambas, T.; Peduzzi, P.; Velegrakis, A.; Chatenoux, B.; Estrella, M.; Karambas, T. Assessment of the Role of Nearshore Marine Ecosystems to Mitigate Beach Erosion: The Case of Negril (Jamaica). *Environments* **2022**, *9*, 62. [\[CrossRef\]](#)



48. Carioli, A.; Schiavina, M.; MacManus, K.J.; Freire, S. GHS-POP R2023A—GHS Population Grid Multitemporal (1975–2030). European Commission, Joint Research Centre (JRC) (Dataset). 2023. Available online: <http://data.europa.eu/89h/2ff68a52-5b5b-4a22-8f40-c41da8332cfe> (accessed on 11 January 2026).
49. Stamatiadou, V.; Mazaris, A.; Sidera, P.; Chalazas, T.; Velegrakis, A.; Katsanevakis, S. Monetary Valuation and Spatial Mapping of Recreational Ecosystem Service Along Greek Coasts. *SSRN* 2024, preprint. [\[CrossRef\]](#)
50. Hellenic Statistical Authority. 2021 Population-Housing Census—ELSTAT. 2021. Available online: <https://www.statistics.gr/en/2021-census-pop-hous> (accessed on 19 March 2024).
51. Bank of Greece. Travel Services. 2022. Available online: <https://www.bankofgreece.gr/en/statistics/external-sector/balance-of-payments/travel-services> (accessed on 19 March 2024).
52. Wood, S.A.; Guerry, A.D.; Silver, J.M.; Lacayo, M. Using social media to quantify nature-based tourism and recreation. *Sci. Rep.* **2013**, *3*, 2976. [\[CrossRef\]](#)
53. WTTC. Monthly Inbound Tourist Arrivals Europe 2023, Statista. 2023. Available online: <https://www.statista.com/statistics/1229666/monthly-change-in-tourist-arrivals-in-europe-coronavirus/> (accessed on 12 January 2024).
54. WTTC. Travel and Tourism GDP Share by Country EU 2022, Statista. 2023. Available online: <https://www.statista.com/statistics/1228395/travel-and-tourism-share-of-gdp-in-the-eu-by-country/> (accessed on 12 January 2024).
55. Stamatiadou, V.; Mazaris, A.D.; Chalazas, T.; Velegrakis, A.F.; Katsanevakis, S. Are beaches accessible to all? Economic valuation and mapping of recreational ecosystem services for wheelchair users in Greece. *Mar. Policy* **2025**, *180*, 106805. [\[CrossRef\]](#)
56. Tzeng, G.-H.; Huang, J.-J. *Multiple Attribute Decision Making: Methods and Applications*; CRC Press: Boca Raton, FL, USA, 2011.
57. Poulter, B.; Halpin, P.N. Raster modelling of coastal flooding from sea-level rise. *Int. J. Geogr. Inf. Sci.* **2008**, *22*, 167–182. [\[CrossRef\]](#)
58. Vousdoukas, M.I.; Voukouvalas, E.; Mentaschi, L.; Dottori, F.; Giardino, A.; Bouziotas, D.; Bianchi, A.; Salamon, P.; Feyen, L. Developments in large-scale coastal flood hazard mapping. *Nat. Hazards Earth Syst. Sci.* **2016**, *16*, 1841–1853. [\[CrossRef\]](#)
59. Sanders, B.F.; Wing, O.E.J.; Bates, P.D. Flooding is Not Like Filling a Bath. *Earths Future* **2024**, *12*, e2024EF005164. [\[CrossRef\]](#)
60. European Space Agency (ESA). Copernicus Digital Elevation Model GLO-30. 2021. Available online: <https://dataspace.copernicus.eu/explore-data/data-collections/copernicus-contributing-missions/collections-description/COP-DEM> (accessed on 11 January 2026).
61. Vousdoukas, M.I.; Mentaschi, L.; Voukouvalas, E.; Verlaan, M.; Jevrejeva, S.; Jackson, L.P.; Feyen, L. Global probabilistic projections of extreme sea levels show intensification of coastal flood hazard. *Nat. Commun.* **2018**, *9*, 2360. [\[CrossRef\]](#)
62. Calvin, K.; Dasgupta, D.; Krinner, G.; Mukherji, A.; Thorne, P.W.; Trisos, C.; Romero, J.; Aldunce, P.; Barrett, K.; Blanco, G.; et al. *IPCC, 2023: Climate Change 2023: Synthesis Report; Contribution of Working Groups I, II and III to the Sixth Assessment Report of the Intergovernmental Panel on Climate Change; Core Writing Team, Lee, H., Romero, J., Eds.; Intergovernmental Panel on Climate Change (IPCC): Geneva, Switzerland, 2023.* [\[CrossRef\]](#)
63. Hausfather, Z.; Peters, G.P. Emissions—The ‘business as usual’ story is misleading. *Nature* **2020**, *577*, 618–620. [\[CrossRef\]](#)
64. Masson-Delmotte, V.; Zhai, P.; Pirani, A.; Connors, S.L.; Péan, C.; Berger, S.; Caud, N.; Chen, Y.; Goldfarb, L.; Gomis, M.I.; et al. (Eds.) *Climate Change 2021: The Physical Science Basis; Contribution of Working Group I to the Sixth Assessment Report of the Intergovernmental Panel on Climate Change; Cambridge University Press: Cambridge, UK; New York, NY, USA, 2021.* [\[CrossRef\]](#)
65. Schwalm, C.R.; Glendon, S.; Duffy, P.B. RCP8.5 tracks cumulative CO2 emissions. *Proc. Natl. Acad. Sci. USA* **2020**, *117*, 19656–19657. [\[CrossRef\]](#)
66. Foteinis, S.; Synolakis, C.E. Beach erosion threatens Minoan beaches: A case study of coastal retreat in Crete. *Shore Beach* **2015**, *83*, 53–62.
67. Monioudi, I.N.; Velegrakis, A.F.; Chatzipavlis, A.E.; Rigos, A.; Karambas, T.; Vousdoukas, M.I.; Hasiotis, T.; Koukourouvli, N.; Peduzzi, P.; Manoutsoglou, E.; et al. Assessment of island beach erosion due to sea level rise: The case of the Aegean archipelago (Eastern Mediterranean). *Nat. Hazards Earth Syst. Sci.* **2017**, *17*, 449–466. [\[CrossRef\]](#)
68. Jenks, G.F. The Data Model Concept in Statistical Mapping. In *International Yearbook of Cartography*; George Philip & Son: London, UK, 1967; Volume 7.
69. Ravdas, M.; Zacharioudaki, A.; Korres, G. Implementation and validation of a new operational wave forecasting system of the Mediterranean Monitoring and Forecasting Centre in the framework of the Copernicus Marine Environment Monitoring Service. *Nat. Hazards Earth Syst. Sci.* **2018**, *18*, 2675–2695. [\[CrossRef\]](#)
70. Litsi-Mizan, V.; Efthymiadis, P.T.; Gerakaris, V.; Serrano, O.; Tsapakis, M.; Apostolaki, E.T. Decline of seagrass (*Posidonia oceanica*) production over two decades in the face of warming of the Eastern Mediterranean Sea. *New Phytol.* **2023**, *239*, 2126–2137. [\[CrossRef\]](#)
71. Ieronymidi, E.; Grigoriadis, D. Guidelines for D3.1—Coastal Dataset Including Exposure and Vulnerability Layers, Deliverable 3.1—ECFAS Project (GA 101004211). 2022. Available online: <https://zenodo.org/records/7313438> (accessed on 11 January 2026).
72. Chatzistratis, D.; Velegrakis, A.F.; Chalazas, T.; Alves, B.; Schiavon, E.; Monioudi, I.N.; Armaroli, C. European Early Warning Systems for coastal floods: User needs, system availability and pertinent policy and legislation. *Int. J. Disaster Risk Reduct.* **2025**, *126*, 105602. [\[CrossRef\]](#)

73. Directive (EU) 2022/2557 of the European Parliament and of the Council of 14 December 2022 on the Resilience of Critical Entities and Repealing Council Directive 2008/114/EC (Text with EEA Relevance). 2022. Available online: [https://eur-lex.europa.eu/legal-content/EN/TXT/?uri=uriserv%3AOJ.L\\_.2022.333.01.0164.01.ENG&toc=OJ%3AL%3A2022%3A333%3AFULL](https://eur-lex.europa.eu/legal-content/EN/TXT/?uri=uriserv%3AOJ.L_.2022.333.01.0164.01.ENG&toc=OJ%3AL%3A2022%3A333%3AFULL) (accessed on 11 January 2026).
74. Vecchio, A.; Anzidei, M.; Serpelloni, E. Sea level rise projections up to 2150 in the northern Mediterranean coasts. *Environ. Res. Lett.* **2024**, *19*, 014050. [[CrossRef](#)]
75. Ohenhen, L.O.; Shirzaei, M.; Ojha, C.; Kirwan, M.L. Hidden vulnerability of US Atlantic coast to sea-level rise due to vertical land motion. *Nat. Commun.* **2023**, *14*, 2038. [[CrossRef](#)] [[PubMed](#)] [[PubMed Central](#)]
76. Thiéblemont, R.; le Cozannet, G.; Nicholls, R.J.; Rohmer, J.; Wöppelmann, G.; Raucoles, D.; de Michele, M.; Toimil, A.; Lincke, D. Assessing Current Coastal Subsidence at Continental Scale: Insights from Europe Using the European Ground Motion Service. *Earth's Future* **2024**, *12*, e2024EF004523. [[CrossRef](#)]
77. Slangen, A.B.A.; Adloff, F.; Jevrejeva, S.; Leclercq, P.W.; Marzeion, B.; Wada, Y.; Winkelmann, R. A review of recent updates of sea-level projections at global and regional scales. In *Integrative Study of the Mean Sea Level and Its Components*; Springer: Cham, Switzerland, 2017; pp. 395–416.
78. Sannino, G.; Carillo, A.; Iacono, R.; Napolitano, E.; Palma, M.; Pisacane, G.; Struglia, M. Modelling Present and Future Climate in the Mediterranean Sea: A Focus on Sea-Level Change. *Clim. Dyn.* **2022**, *59*, 357–391. [[CrossRef](#)]

**Disclaimer/Publisher's Note:** The statements, opinions and data contained in all publications are solely those of the individual author(s) and contributor(s) and not of MDPI and/or the editor(s). MDPI and/or the editor(s) disclaim responsibility for any injury to people or property resulting from any ideas, methods, instructions or products referred to in the content.